AD-A070 080 FLORIDA UNIV GAINESVILLE DEPT OF ENGINEERING SCIENCES F/G 20/9
HARTMANN FLOWS IN THE MHD GENERATOR CONFIGURATION.(U)
JUN 79 R E ELKINS, T A TROVILLION N00014-76-C-0410
UNCLASSIFIED TR-01-002 NL

| OF |
AD
A070080

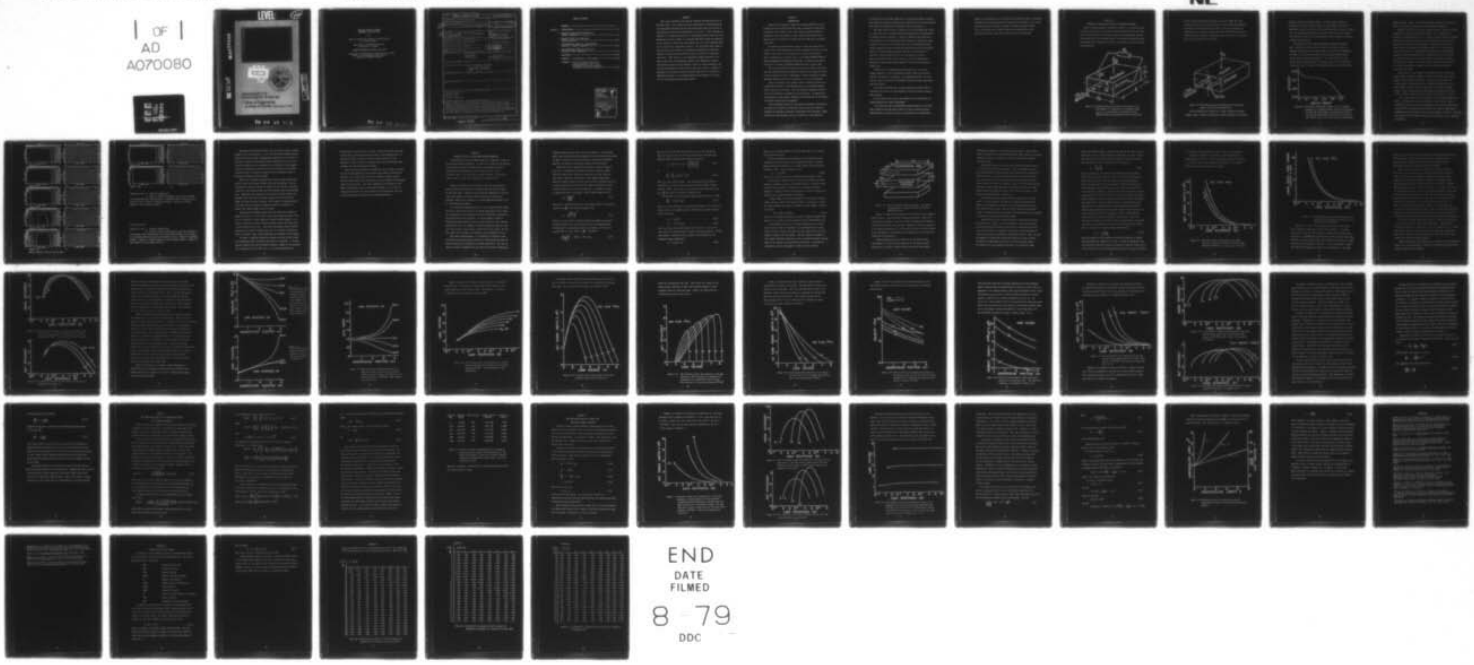

END
DATE
FILMED
8-79
DDC

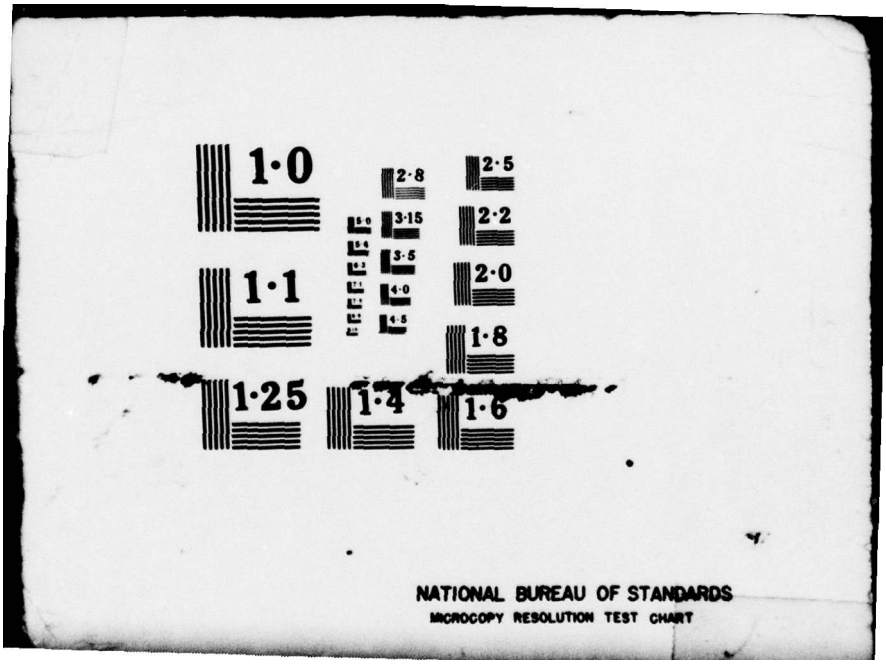
1·0
1·1
1·25
2·8
3·15
3·5
4·0
4·5
2·5
2·2
2·0
1·8
1·4
1·6
NATIONAL BUREAU OF STANDARDS
MICROCOPY RESOLUTION TEST CHART

LEVEL II

12

AD A070080

DDC FILE COPY

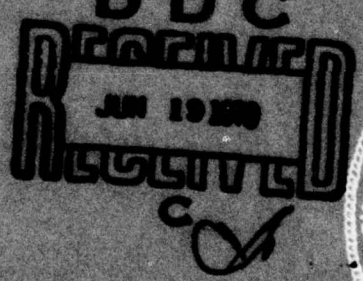

DEPARTMENT OF
ENGINEERING SCIENCES
College of Engineering
University of Florida Gainesville, FL 32611

79 06 18 013

HARTMANN FLOWS IN THE MHD GENERATOR CONFIGURATION

by

Rush E. Elkins III, Thomas A. Trovillion and
E. Rune Lindgren

Department of Engineering Sciences
University of Florida

TECHNICAL REPORT NR 01-002, June 1979

Final Report on MHD Research Sponsored by U.S. Navy
Office of Naval Research, Power Branch
Contract No N00014-76-C-0410

SECURITY CLASSIFICATION OF THIS PAGE (When Data Entered)

REPORT DOCUMENTATION PAGE

READ INSTRUCTIONS BEFORE COMPLETING FORM

1. REPORT NUMBER: Department of Engineering Sciences Univ. of Florida Technical Report
2. GOVT ACCESSION NO.
3. RECIPIENT'S CATALOG NUMBER

4. TITLE (and Subtitle) 01-002
(6) Hartmann Flows in the MHD Generator Configuration

5. TYPE OF REPORT & PERIOD COVERED
(9) Technical rept.,

6. PERFORMING ORG. REPORT NUMBER

7. AUTHOR(s)
(10) Rush E. Elkins, III, Thomas A. Trovillion and E. Rune Lindgren

8. CONTRACT OR GRANT NUMBER(s)
(15) N00014-76-C-0410

9. PERFORMING ORGANIZATION NAME AND ADDRESS
Department of Engineering Sciences, College of Engineering, University of Florida
Gainesville, Florida 32611

10. PROGRAM ELEMENT, PROJECT, TASK AREA & WORK UNIT NUMBERS
TASK NO. NR 099-412

11. CONTROLLING OFFICE NAME AND ADDRESS
Power Program, Material Sciences Division
Office of Naval Research
800 N. Quincy St. Arlington, Virginia 22217

(11)

12. REPORT DATE
June 1979

13. NUMBER OF PAGES
56

14. MONITORING AGENCY NAME & ADDRESS (if different from Controlling Office)
(12) 64p.

15. SECURITY CLASS. (of this report)
Unclassified

15a. DECLASSIFICATION/DOWNGRADING SCHEDULE

16. DISTRIBUTION STATEMENT (of this Report)

Approved for public release; distribution unlimited.

(14) TR-01-002

17. DISTRIBUTION STATEMENT (of the abstract entered in Block 20, if different from Report)

18. SUPPLEMENTARY NOTES

19. KEY WORDS (Continue on reverse side if necessary and identify by block number)
Magnetohydrodynamics
Two-Phase Flows
Hartmann Flows
MHD Power Generators

20. ABSTRACT (Continue on reverse side if necessary and identify by block number)
Specific features and characteristics of Hartmann flows in the Faraday generator configuration are reported. These features concern the effect of longitudinal baffling along the insulating duct walls, effects of slip between gas-liquid phases in the flow. The report also contains an analysis of a compensating system of a Faraday generator as well as a one-dimensional zero-slip model of a two-phase MHD flow through the generator.

DD FORM 1 JAN 73 1473 EDITION OF 1 NOV 65 IS OBSOLETE

Unclassified LB

SECURITY CLASSIFICATION OF THIS PAGE (When Data Entered)

410 049

TABLE OF CONTENT

ABSTRACT

This report documents some specific features and characteristics of Hartmann flows in the Faraday generator configuration concerning effects of longitudinal baffling along the insulating duct walls and, effects of slip between gas-phase and liquid-phase in the flow. It also contains an analysis of a compensating system of a Faraday generator as well as a one-dimensional zero-slip model of a two-phase MHD flow through the generator. Of the results we notice that there appears not to be any efficiency gain by the insertion of longitudinal baffles. The slip model again seems to over predict the performance of experimental generators by typically fifteen to twenty percent within the range of validity for approximations made. With respect to the compensated Faraday generator we are able to show that one-dimensional models cannot adequately represent interactions between flow and magnetic field in a finite generator, but that three-dimensional effects must be taken into account. Finally, an expression is derived for channel cross-section area as a function of downstream distance to give optimum generator performance in the case of zero slip between gas and liquid phases.

Chapter 1

INTRODUCTION

Analytical and numerical studies on two-phase MHD-flows in the Faraday generator configuration have been in progress at University of Florida since December, 1975. The studies have been aimed as a complement to the experimental efforts that have been under way at Argonne National Laboratory on liquid metal-gas MHD power generation since 1969.

The efforts during the first couple of years were directed towards a better understanding of the basic principles involved in these types of flows and to try to model some of these flow processes. This is reflected by an annual report on TWO PHASE HARTMANN FLOWS IN THE MHD GENERATOR CONFIGURATION, Department of Engineering Sciences, University of Florida, TECHNICAL REPORT NR 01-001, January 1978.

The continued efforts thereafter have been directed towards more specific problems which have presented themselves as urgent and being of vital interest in view of experimental results obtained at Argonne National Laboratory and lack of analytical data in the literature.

Thus, one section of the present report concerns the effects of longitudinal baffling of the generator duct as to prevent Hartmann layer current short circuits. This was deemed an important issue in view of contradictory statements in the literature. It appears our contribution on this subject (submitted for publication in the Physics of Fluids) should settle the dispute.

One of the main sections of the report is devoted to the effects of slip upon the generator performance and how well the numerical analysis can represent and predict experimental data obtained. While there still exist enormous gaps in the modeling of the behaviour

of voids in the liquid metal MHD flows, the presented computer modeling does give much valuable information both quantitatively and qualitatively with regard to experimental findings and their interpretation.

The report also contains an analysis of an "one-dimensional" model of a generator and its compensating system utilized for experimentation at Argonne National Laboratory. While the computer model shows that the assumption of a uniform applied flux density is satisfied to quite a degree of accuracy it also shows that truly one-dimensional models cannot adequately estimate interactions between fluid flow and magnetic field in a finite Faraday generator. However, we have managed to develope an averaged Ampere's Law over the Hartmann generator duct cross-section which can be used for sorts of one-dimensional modeling of interactions between magnetic field and the conducting liquid flow.

Finally, we have investigated the properties of a zero-slip Faraday generator by an one-dimensional model, which then has been used for the design of a generator of optimum performance all along its duct length for several relationships between average conductivity and void fraction.

This report concludes our research program on two-phase MHD as directed by the Office of Naval Research, Material Sciences Division, Power Program.

Here we would like to add a few comments on the potentiality of Faraday machines for future development.

It is true that the two-phase MHD Faraday generators of the kind that presently have been under study by us and at Argonne National Laboratory may not seem to harbor vast possibilities of improvement.

However, the performance of such machines may possibly permit considerable improvement by subpartitioning the channel duct as proposed in the report mentioned previously (Elkins, Kurzweg, Trovillion, Lindgren, 1978). It is our feeling that a limited study of the feasibility of such MHD generators may produce interesting results and conclusions.

Chapter 2

EFFECTS OF LONGITUDINAL BAFFLING IN FARADAY GENERATORS

When a Faraday generator, sketched in Figure 2.1, is operated with a nonzero load, part of the electric current generated by the core flow will return through the load and part will return through the Hartmann layers adjacent to the insulating walls. The current returning through the Hartmann layers represents a loss to the system, since it cannot be used externally.

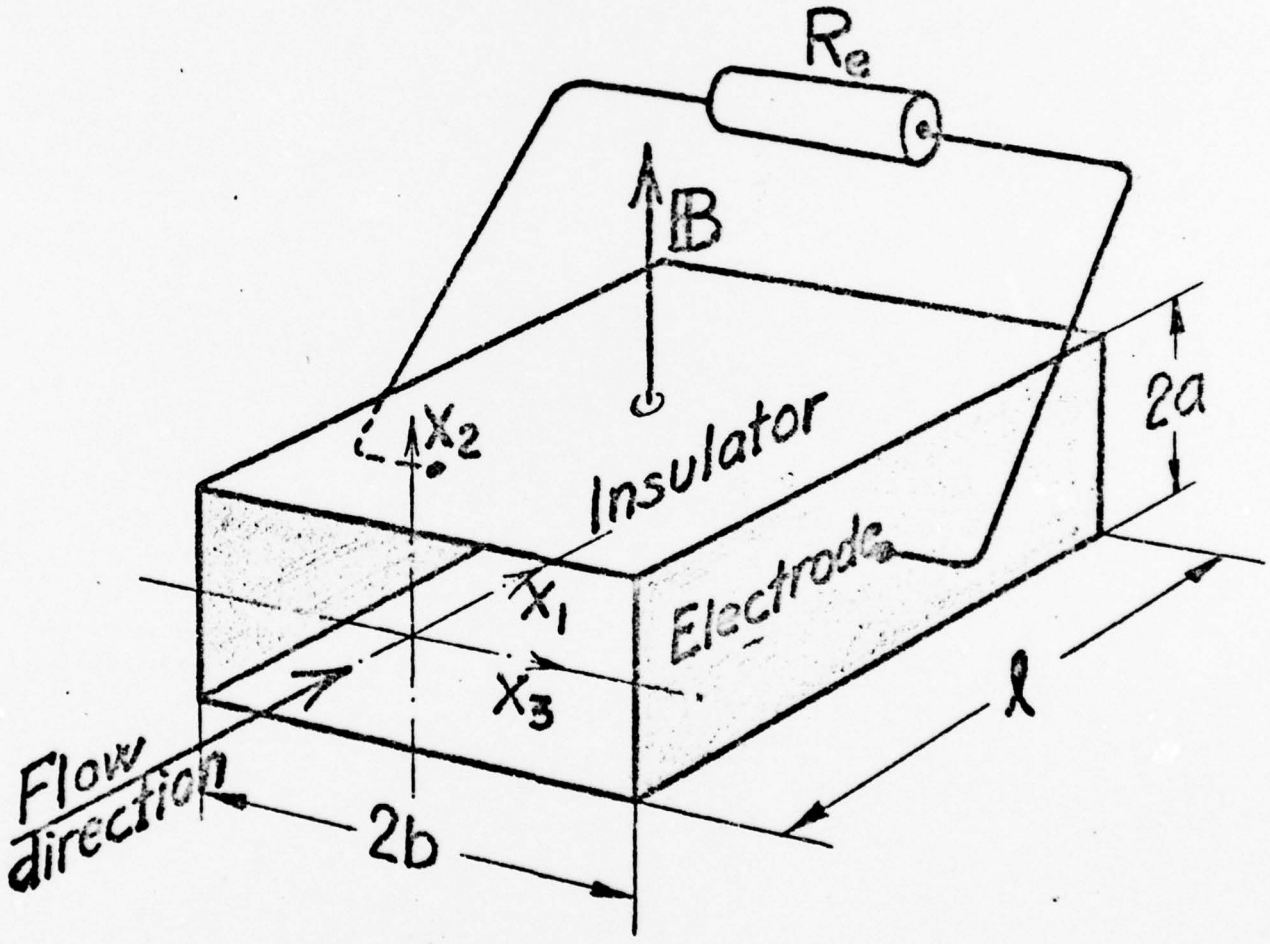

Figure 2.1- Faraday generator of length ℓ, half-width b and half-height a as oriented in the reference frame x_1, x_2, x_3. B indicates the direction of the magnetic field and R_e symbolizes the external load.

It has recently been suggested (Yakhot and Levin, 1978) that this electric current can be attenuated and the system efficiency improved by inserting insulating baffles parallel to the flow along the insulating walls. On the other hand, Shercliff (1977) found that such baffles will not interrupt the Hartmann current and that no efficiency gain can be obtained in this fashion.

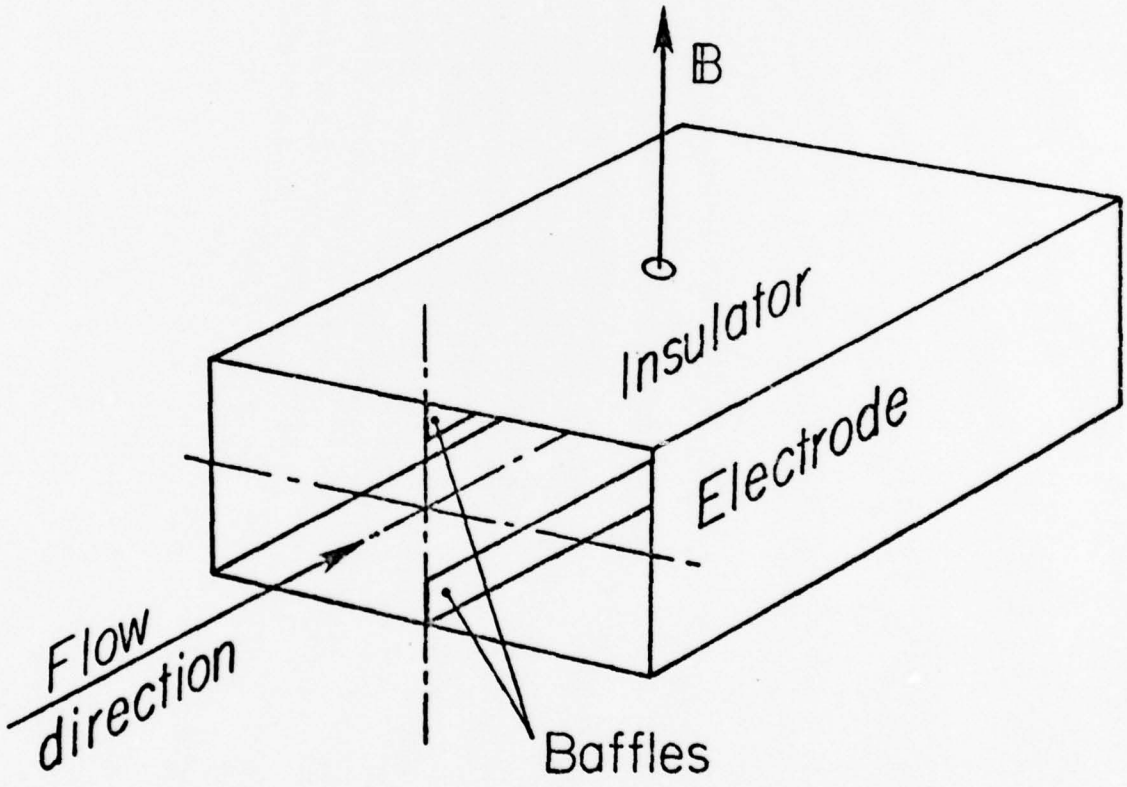

Figure 2.2- The Faraday generator equipped with longitudinal baffles along the insulating walls.

We have examined the problem for a range of moderate Hartmann numbers, using a numerical integration scheme described by Trovillion,

Kurzweg, Elkins and Lindgren (1979). In these computer model experiments, we placed vertical baffles of zero thickness and various heights along the center lines of the insulating walls as shown in Figure 2.2. The program generated plots of current and velocity streamlines and listings of power and efficiency which could be compared to similar systems without baffles.

The results of these computer experiments support Shercliff's work. Inserting a baffle into the flow in all cases was found to decrease the efficiency by a small amount. This effect is summarized in Figure 2.3 where the efficiency is plotted versus baffle height for two sets of operating parameters. It can be seen that, as the baffle height protrudes across the Hartmann layer, the efficiency decreases to a fairly constant level slightly below that for the channel

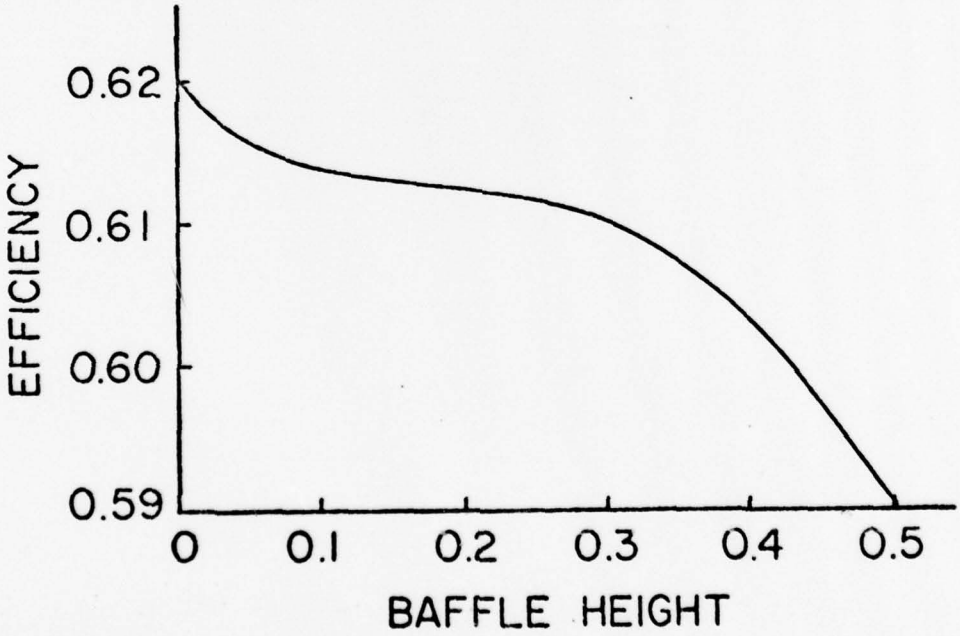

Figure 2.3- Efficiency versus baffle height for a 2:1 Faraday generator at a Hartmann number of 20 and a load factor of 0.82. The baffle height is specified in terms of half channel height.(The load factor is the ratio of the external, R_e, to the total electrical resistance.)

without baffles. Then, as the baffle protrudes further, into the core flow, the efficiency again begins to decrease more markedly.

Figures 2.4a and 2.4b are first quadrant plots of constant velocity contours and of electric current streamlines for an unbaffled, 2:1 channel at a Hartmann number of 20. There is an equal velocity increment between each velocity contour and an equal amount of electric current flowing between each current streamline. Figures 2.9a and 2.9b are plots for the same channel at a Hartmann number of 40. The Hartmann layer in these plots is delineated by the regions of closely packed contours along the insulating walls in Figures 2.4a and 2.9a and by the near wall portions of the closed current streamlines in Figures 2.4b and 2.9b. Figures 2.5 through 2.8 and 2.10a and 2.10b show how the velocity and electric current fields are affected as baffles extend into the flow.

With baffles of small height, the Hartmann layer is simply displaced around the baffle (Figures 2.5a, 2.6a and 2.10a) with a small change in the velocity at the core. A portion of the current returning through the Hartmann layer is likewise deflected around the baffle (Figures 2.5b, 2.6b and 2.10b), with the remainder looping around to form a closed current loop between the baffle and the electrodes. Such a structure does not exist in the absence of a baffle.

On the other hand, the net percentage of current flowing past the baffle is changed little by the presence of a small baffle. This is reflected in the fact that the distribution of current streamlines along the electrode is changed little and in the fact that the same number of streamlines pass the channel center with and without the baffle. Similarly, the structure of the current streamlines in the channel core is virtually unperturbed.

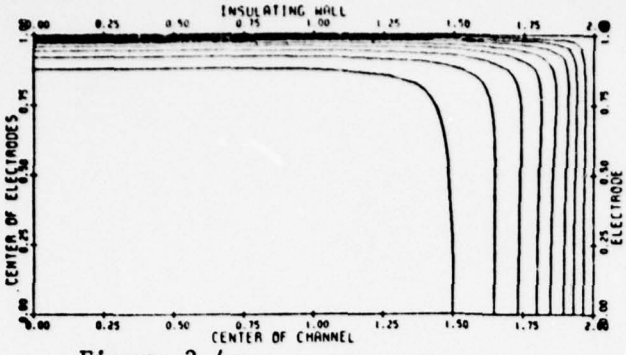

Figure 2.4a

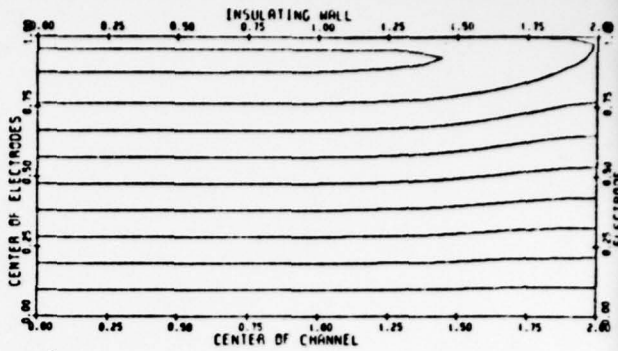

b.

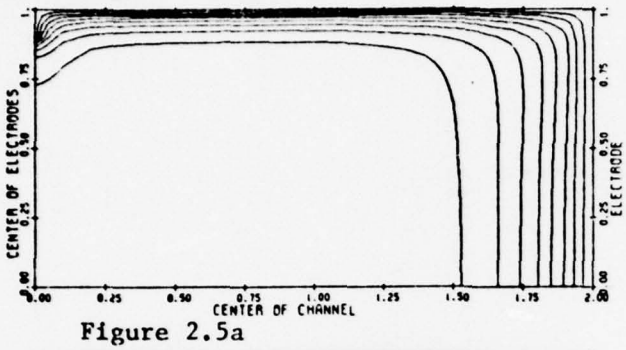

Figure 2.5a

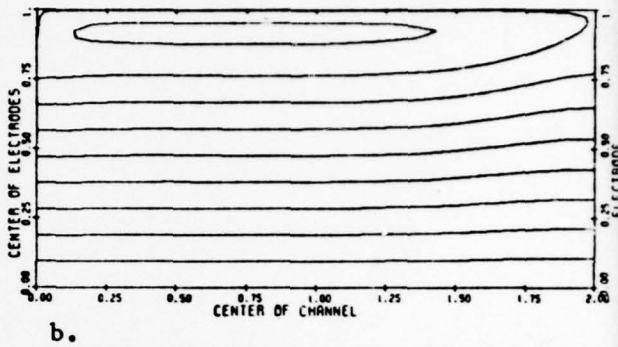

b.

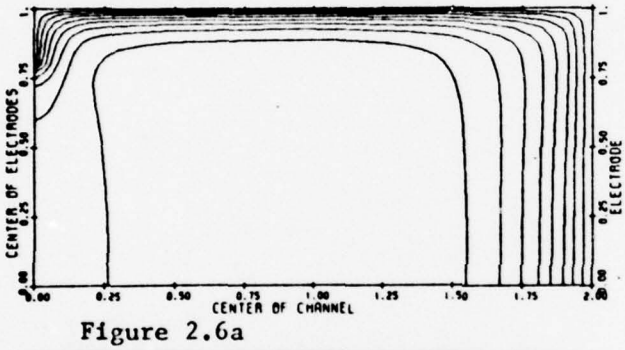

Figure 2.6a

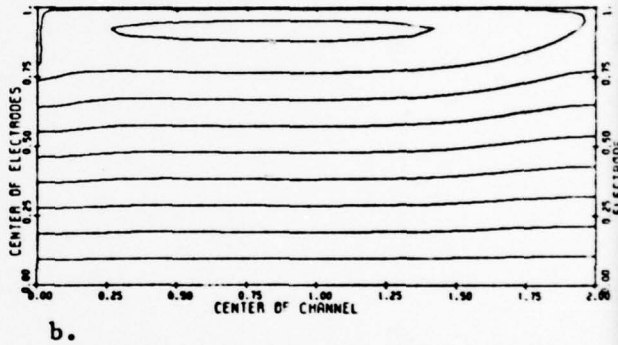

b.

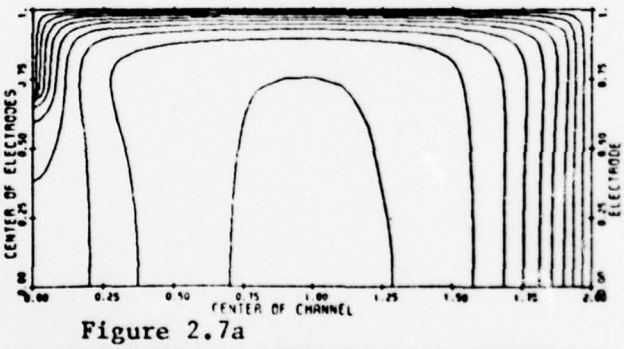

Figure 2.7a

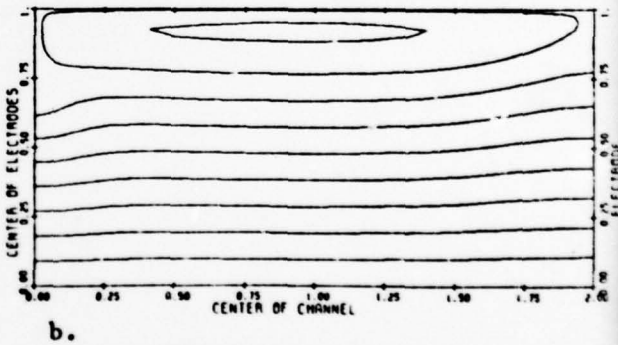

b.

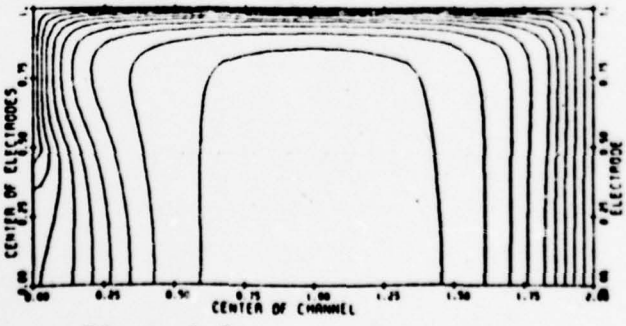

Figure 2.8a

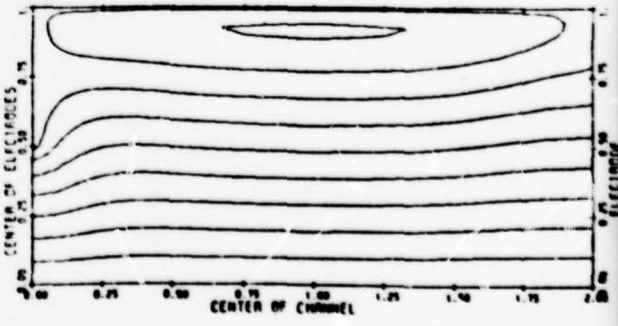

b.

Text to Figures 2.4-2.8; See next page.

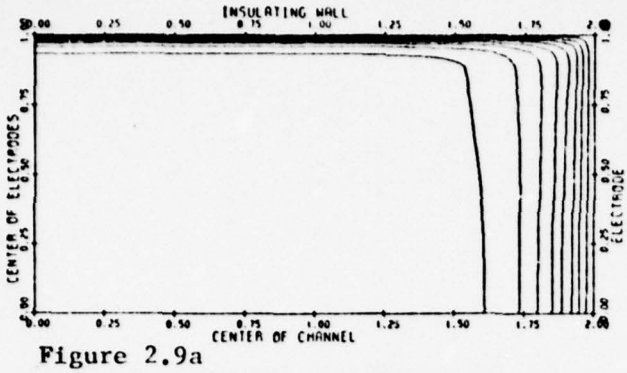

Figure 2.9a

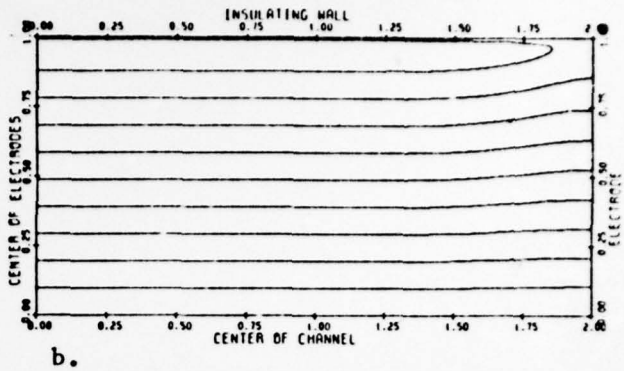

b.

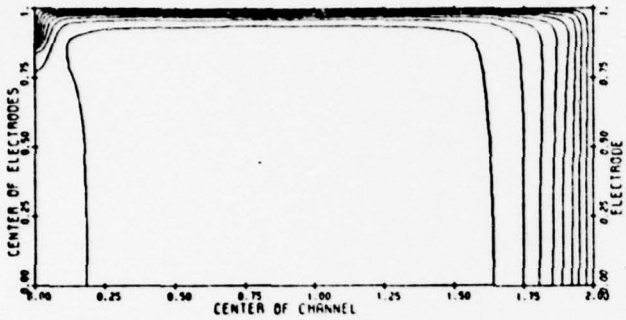

Figure 2.10a

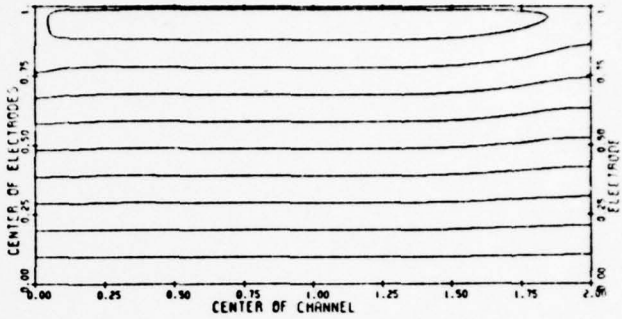

b.

Figures 2.9-2.10 a. Velocity contours and

b. Electric current streamlines in the first quadrant of the generator duct cross section at a Hartmann number of 40 and a load factor of 0.86. Figure 2.9: Unbaffled channel. Figure 2.10: Baffle height 0.1 of half channel height.

For previous page--

Figures 2.4-2.8- a. Velocity contours and

b. Electric current stream lines in the first quadrant of the generator duct cross section for various baffle heights in the channel at a Hartmann number of 20 and a load factor of 0.82. Figure 2.4: Unbaffled channel. Figure 2.5: Baffle height 0.1 of half channel height. Figure 2.6: 0.2; Figure 2.7: 0.3; Figure 2.8: 0.5.

Extension of the baffles further into the channel leads to marked changes in the flow structure. A low velocity region extends from the baffle into the core flow, becoming more pronounced as the baffle approaches a quarter of the channel height (Figures 2.5a, 2.6a, 2.7a). It may be thought of as an extension in the direction of the magnetic field of the perturbed velocity field in the vicinity of the baffle. A similar effect occurring in large interaction parameter flows is described by Hughes and Young (1966).

While core streamlines undergo deflections as they approach the baffles, they are not much affected away from the baffles. The net percentage of current crossing the channel is for the case of baffles a quarter of the channel height not much different from the unbaffled case. Similarly, the structure of the electric current field in the Hartmann layer away from the baffles changes little as the baffle height increases, but the thickness of the region of reversed current flow (away from the baffle) is nearly the same for a baffle of a quarter the channel height as for no baffle.

Those current streamlines which pass the baffle are crowded together as they do so. This effect can be seen clearly in Figure 2.7b, but it is present in lesser degree for smaller baffle heights. As a result, the electric current density is greater above the baffle than in other regions of the core. The region with higher current density experiences an excess retarding force and, as a result, the velocity there is reduced. Also, ohmic dissipation is increased in this region.

In short, a baffling system will neither block the return current in the Hartmann layer nor improve the generator efficiency. A no slip viscous condition for solid boundaries implies a region of low velocity and, consequently, of low EMF, next to the insulating boundaries

through which a return current can flow. Note that one may also look at the return current as driving the fluid in the Hartmann layer, so bringing the high velocity of the core region in nearer to the boundaries. This is seen as a Hartmann layer velocity gradient which steepens with increasing Hartmann number.

Yakhot and Levin (1978) err in supposing that a baffle can change the current distribution of the Hartmann layer without affecting the velocity. The current and velocity are strongly coupled, and the velocity field changes just sufficiently so as to maintain the Hartmann layer electric current. But, while moderately sized baffles do not improve efficiency, neither do they much degrade it. If it is for some reason desirable to insert baffles into the generator, they can be inserted without much lowering the system performance.

Chapter 3

EFFECTS OF SLIP IN A TWO-PHASE FARADAY GENERATOR

Slip between the gas and liquid phases is an important feature of the two phase Faraday generator. It arises as a result of the Lorentz force acting solely on the liquid phase, so creating a pressure gradient in the liquid phase, and a "bouyancy force" on any entrained voids. The voids must then move relative to the liquid phase in such a fashion as to balance this bouyancy force.

Except at extremes of void fraction, there are presently no purely analytic descriptions of two phase flow (see Wallis, 1969). On the other hand, a number of well documented semiempirical descriptions exist which, as noted by Elkins, Kurzweg, Trovillion and Lindgren (1978), may be applied to two phase magnetohydrodynamic flow in a straightforward manner.

If a two phase Faraday generator is run at large Hartmann number, and if the liquid velocity does not change appreciably in the length of the generator, then viscosity and inertia contribute negligibly to the downstream pressure gradient. In the generators studied at Argonne National Laboratory (Petrick, Fabris, Pierson, Curl, Fischer and Johnson, 1977), for example, viscosity dissipates generally less than five percent of the mechanical work done by the fluids. By far, the largest force acting on the liquid is the ponderomotive force.

With these considerations, it is possibly to construct a simplified force and mass balance suitable for describing such flows as those encountered in experimental two-phase generators. For now, we make the further assumption that the system is perfectly compensated

(Jackson, 1963) and that there are no end currents. The resulting model, while preserving the most important force and energy mechanisms, is simple enough to provide descriptions of flow in the two-phase generator via numerical integration quickly and efficiently.

While flow in the experimental generators cannot be observed directly, it probably moves within the "churn" turbulent regime (Petrick, Fabris, Cole, Hartmann, Pierson and Cutting, 1976; see also Wallis, 1969 for a discussion of flow regime transitions). Zuber and Findlay (1965) note that voids in churn turbulent flow move at rates characteristic of bubbly flow voids, but relative to the average volumetric velocity of the mixture. It remains to choose an appropriate bubbly flow model. Wallis (1969) suggest that if

$$R_B \geq 2\left(\frac{\gamma}{\frac{\partial P}{\partial x}}\right)^{\frac{1}{2}} \tag{3.1}$$

where R_B is a size characteristic of the bubble radius, γ is surface tension, and $\frac{\partial P}{\partial x}$ is the pressure gradient, then

$$u_\infty = \left(\frac{\frac{\partial P}{\partial x} R_B}{\rho}\right)^{\frac{1}{2}} \tag{3.2}$$

where u_∞ is the relative velocity between the bubble and its surrounding medium, and ρ is the density of the surrounding medium. We take 0.01 m as a probably size for the bubbles, 0.1 N/m for γ, and 10^5 N/m^3 as a lower limit on $\frac{\partial P}{\partial x}$. This gives

$$2\left(\frac{\gamma}{\frac{\partial P}{\partial x}}\right)^{\frac{1}{2}} = .002 \text{ m} < .01 \text{ m} = R_B \tag{3.3}$$

Now, if u_L is the average liquid velocity, u_G is the average gas velocity, and α is the void fraction, then we have from Zuber and Findlay's (1965) suggestion and equation (3.2) that

$$u_a - (u_L(1-\alpha) + u_G\alpha) = \left(\frac{\frac{\partial P}{\partial x} R_B}{\rho_L(1-\alpha)} \right)^{\frac{1}{2}} \tag{3.4}$$

or

$$\frac{\partial P}{\partial x} = \frac{\rho_L}{R_B} (u_G - u_L)^2 (1-\alpha)^3 \tag{3.5}$$

where ρ_L is the liquid density. This semiempirical slip model is essentially the same as that described by Petrick, Amend, Pierson and Hsu, (1970). Note that it loses validity for sufficiently small R_B or $\frac{\partial P}{\partial x}$, and also for non-churn turbulent flow.

We also have the force balance equation (see Elkins et al 1978)

$$\frac{\partial P}{\partial x} = -\sigma B(E + u_L B) \tag{3.6}$$

where σ is the conductivity of the dispersed liquid, E is the electric field, and B is the applied magnetic flux density, and the two mass balance equations

$$q_G = \alpha u_G AkP \tag{3.7}$$

$$q_L = (1-\alpha) u_L A\rho_L \tag{3.8}$$

where q_G and q_L are gas and liquid mass flow rates. A is channel area, and k is a proportionality constant relating pressure, P, and gas mass density. Finally we have to specify some relation for the dispersed liquid conductivity

$$\sigma = \sigma_L f(1 - \alpha) \tag{3.9}$$

where σ_L is the conductivity of the pure liquid and f is a function of the liquid fraction.

Several semiempirical relationships for the dispersed liquid conductivity have been used in the experimental effort at Argonne National Laboratory (Petrick et al. 1970; Amend, Cole, Cutting and Pittenger, 1973). In our analysis we use

$$\sigma = \sigma_L (1-\alpha)^2 \tag{3.10}$$

since it is close to the cited relationships and simpler in form.

The system of equations (3.5), (3.6), (3.7), (3.8), and (3.10) comprise a complete set, once a functional form for A has been chosen and E has been specified. We chose, for our initial numerical modeling, a channel with the same dimensions as the, so called, LT-3 channel used at Argonne National Laboratory.

A large number of runs are documented for this device (Petrick, Fabris, Pierson, Fischer and Johnson, 1978). Its length is 0.385 m, its width (between electrodes) is 0.1016 m, and its height in meters is given by

$$2h = 0.0141 + 0.0129x \tag{3.11}$$

where x is the downstream distance in meters along the channel axis. Figure 3.1 is a sketch of this generator and its compensating bars.

We programmed the system of governing equations to be solved interactively in APL (see Appendix 1 for documentation) for given values of inlet pressure, gas (N_2) and liquid (NaK) mass flow rates, terminal voltage, and flux density. The APL coding is designed so that channel operating conditions as well as channel geometry and slip model can be quickly and conveniently manipulated. Provisions for nonconstant electric and magnetic fields are also included.

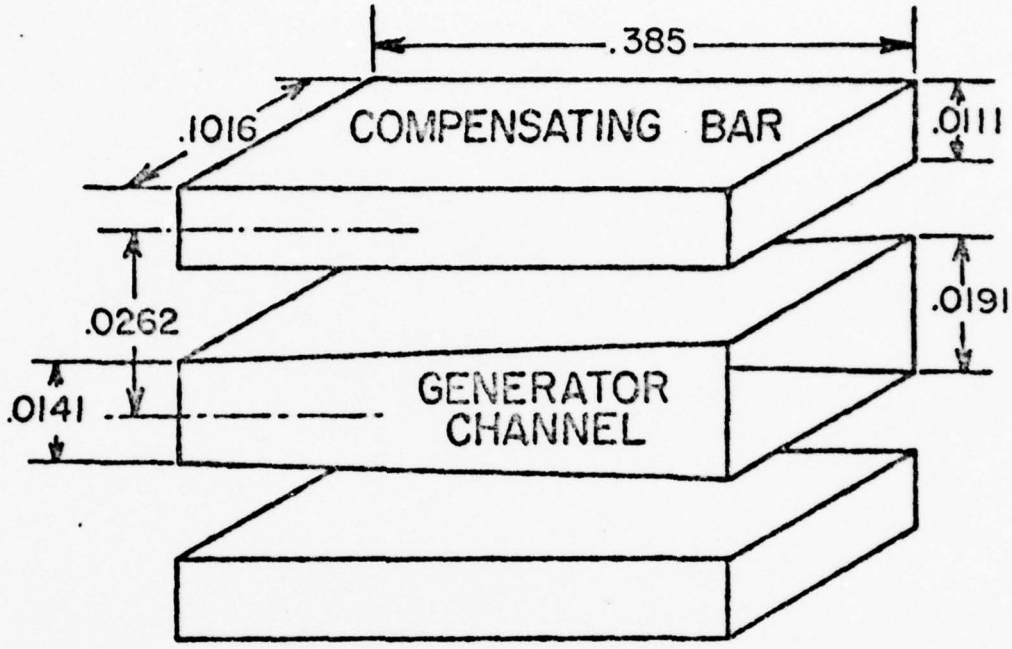

Figure 3.1- The LT-3, N_2-NaK, Faraday generator and compensating system, at Argonne National Laboratory. Measurements in m.

Figures 3.2 through 3.20 represent several "runs" by the computer model generator under different operating parameters. Before discussing these diagrams, a note is in order concerning the interpretation of efficiency for these systems. Compare the two phase generator to an isothermal expansion of a fixed mass of gas in a cylinder closed at one end against a frictionless piston coupled to an ideal (conventional) electric generator.

Finite conductivity of the liquid in the two phase system corresponds to a less than ideal generator in the piston system. Losses occur as electric current passes through the liquid phase

(through the windings of the conventional generator). These losses could be minimized with large Hartmann number, high voltage, and optimal loading and could, in principle, be held to a few percent (Hughes and Young, 1966).

Nonuniform velocity in the two phase system will always lead to a less than optimal loading condition. This is analogous to two or more piston/generator systems connected in parallel, but operating at different speeds. The faster generators will to some extent drive the slower ones, with the result that both fast and slow generators operate under less than ideal loading. Thus, in the two phase system, the faster moving liquid generates power partly to drive the slower moving liquid with additional Joule losses in both processes. This point is discussed further in Chapter 5.

Slip losses in the two phase system are analogous to a leaky piston. As gas leaking by the piston no longer works against the piston, gas slipping by a liquid particle no longer works against that portion of the liquid. Both processes represent irrecoverably losses. Two phase slip losses increase with increasing pressure gradient and increasing void fraction (Wallis, 1969).

Several matters bear on the definition of efficiency of the two phase generator. First, the cycle efficiency cannot be determined without specifying the manner in which heat is rejected from the gas. One can only calculate a component efficiency for the generation of electric power from a reservoir of high pressure fluid. Next, the work of pumping the liquid phase from outlet pressure to inlet pressure represents an appreciable portion of the system's energy budget. Two schemes have been suggested (Petrick et al, 1970) that might

supply this pumping energy. One would use part of the power from the generator to run an electromechanical or MHD pump. In such a system, the useful power available from the generator is the total power P_T less the pump power P_P. We define a net efficiency η_n

$$\eta_n = \frac{P_T - P_P}{P_G + P_P} \tag{3.12}$$

where P_G is the power available in expanding the gas isothermally between the inlet and outlet pressures. It is clear from equation (3.12) that a high net efficiency demands that P_P be minimized, either by decreasing the relative amount of liquid (increasing the void fraction) or by narrowing the relative difference between the inlet and outlet pressures. Another scheme would accelerate the gas/liquid mixture in a nozzle after it has left the generator and subsequently convert to pressure energy the kinetic energy thus imparted to the liquid phase. More work must be done in recompressing the gas phase than in the previous system, and the liquid must be pumped through a larger head, but if the nozzle extracts power from the gas more efficiently than does the generator, then a nozzle/diffuser system may be more efficient overall. We note that, since void fractions are larger in the nozzle than in the generator, slip losses are likely to be larger in the nozzle than in the generator (Wallis, 1969). In any case, we define a gross efficiency η_g

$$\eta_g = \frac{P_T}{P_G + P_P} \tag{3.13}$$

which corresponds to the generator efficiencies reported at Argonne National Laboratory (Amend et al, 1973). It must be remembered that relatively more electrical power is required to pump the fluids in the nozzle system than in the electromechanical system, and η_g is therefore

an imcomplete characterization of energy usage in the generator.

Figures 3.2 through 3.12 illustrate channel operation at a liquid mass flow rate of 15 kg/s, an applied constant flux density of 1.2 Tesla, and an inlet pressure of $6.10^5 N/m^2$. The nitrogen mass flow rate varies from 0.2 to 0.3 kg/s.

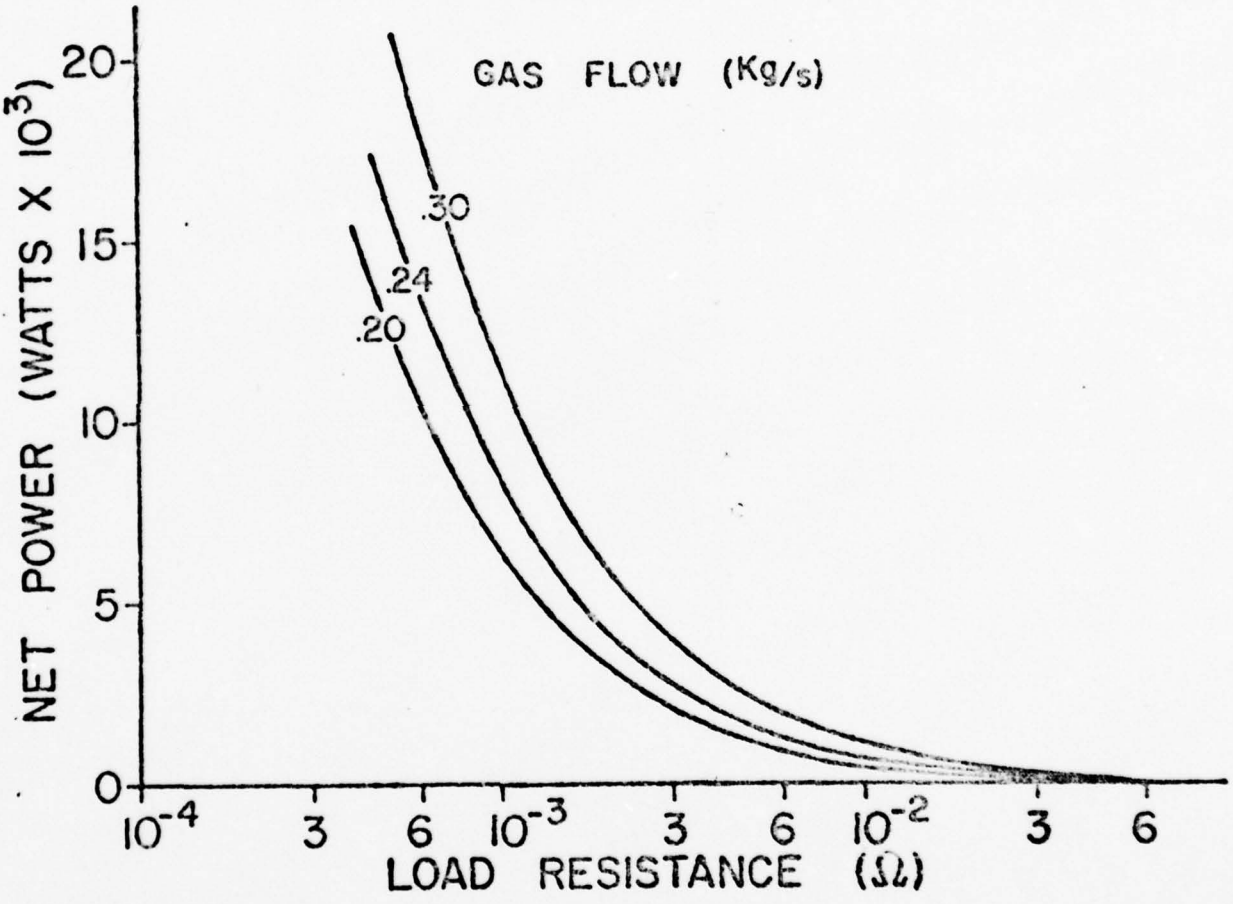

Figure 3.2- Net power versus load resistance for liquid flow rate 15 kg/s; flux density 1.2 T; and inlet pressure $6\text{-}10^5$ N/m^2; and various gas flow rates.

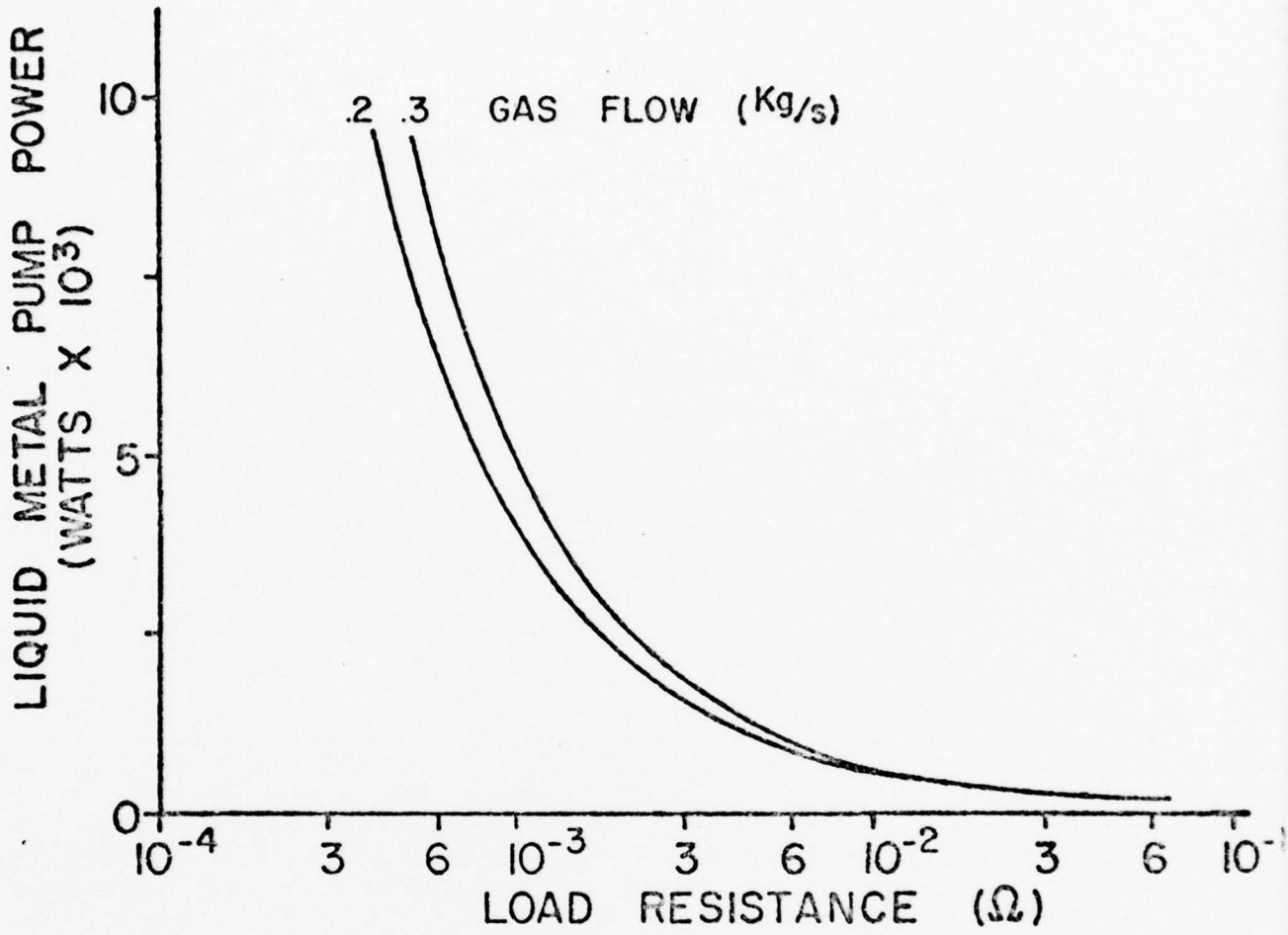

Figure 3.3- Liquid pump power versus load resistance for liquid flow rate 15 kg/s; flux density 1.2 T, inlet pressure 6.10^5 N/m^2.

Figure 3.2 is a plot of net power (electrical power delivered minus liquid metal pump power) versus load resistance. At higher power levels, the net power decreases rapidly with increasing load resistance. Increasing the gas flow rate has the effect of increasing the power level for a given load. This reflects the increase in liquid velocity with increasing gas flow rate. It is interesting to compare the liquid metal pump power, Figure 3.3, with Figure 3.2. The pump

power can be seen to increase with increasing net power and decreasing load resistance. This occurs since the heavier loading leads to a steeper pressure gradient in the channel and a larger pressure differential which the liquid must be pumped through.

Figure 3.4 is a plot of gross efficiency vs. load resistance. Note that the peak efficiency is between 85% and 90% for the entire range of gas flows. This compares to peaks of around 50% to 60% reported for experimental generators operating at Argonne National Laboratory under similar conditions (Petrick et al, 1978). Hartmann layer dissipation accounts for the discrepancy. Peak gross efficiencies in the mathematical model occur for very lightly loaded generators and low power outputs (see Figures 3.4 and 3.5). With similar loading, a real generator would experience viscous and Joule dissipation in the Hartmann layer comparable to the power delivered to the load. In order to overcome the Hartmann layer losses, a real generator must be run at a relatively high power level. Thus, we find the experimental generators at Argonne National Laboratory peaking in gross efficiency at heavier loads than are indicated by the inviscid model presented here.

For heavier loading, the inviscid model is a much better predicter of the performance of the experimental generators. When loading and input parameters are simulated for such cases (Petrick et al, 1978), overall power levels are much larger than Hartmann layer dissipation. Under these conditions, the model overpredicts the gross power output typically by fifteen to twenty percent.

Figure 3.5 shows the net efficiency as a function of load resistance. These curves can be generated, roughly, by multiplying the gross efficiencies of Figure 3.4 by constants.

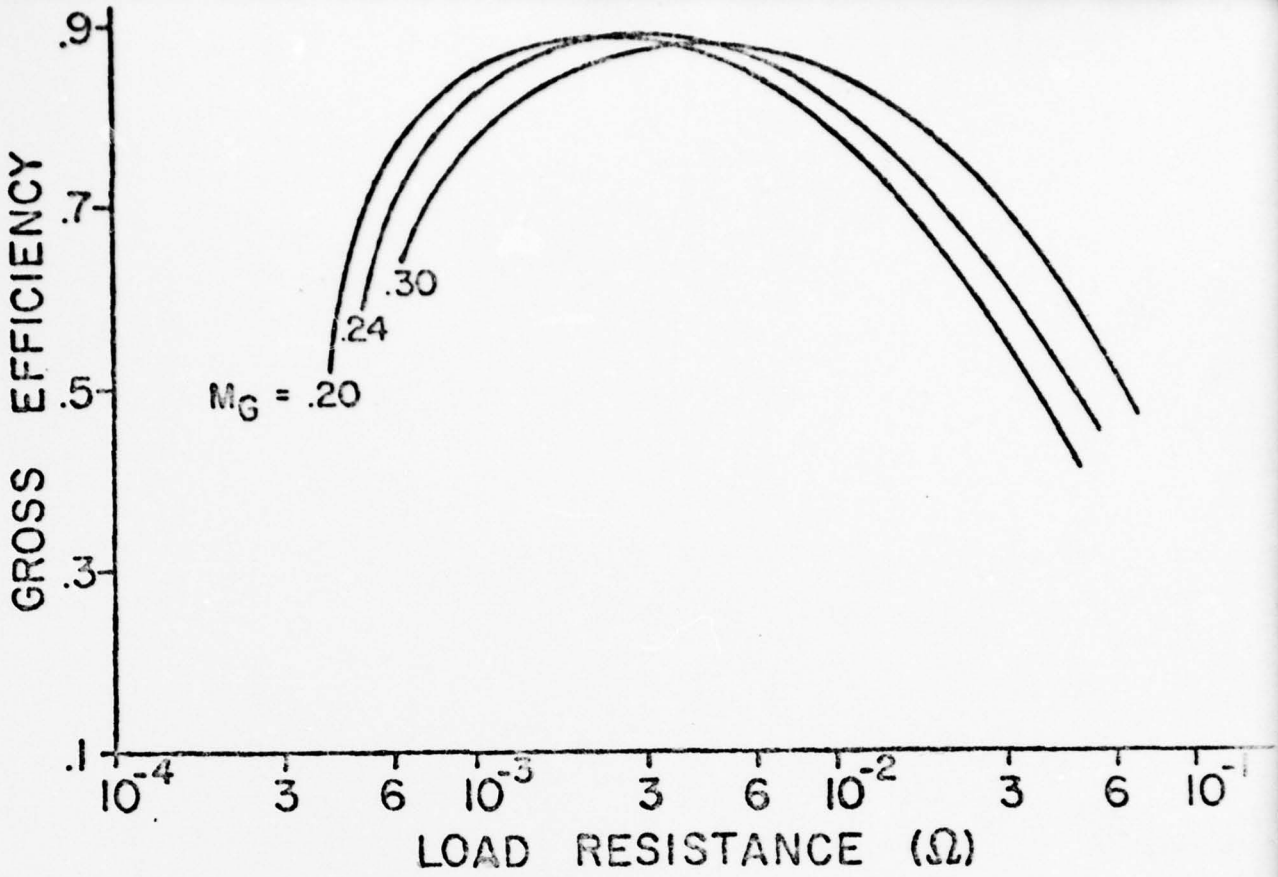

Figure 3.4- Generator gross efficiency versus load resistance for liquid flow rate 15 kg/s; flux density 1.2 T; inlet pressure 6.10^5 N/m^2. M_G is the gas flow rate in kg/s.

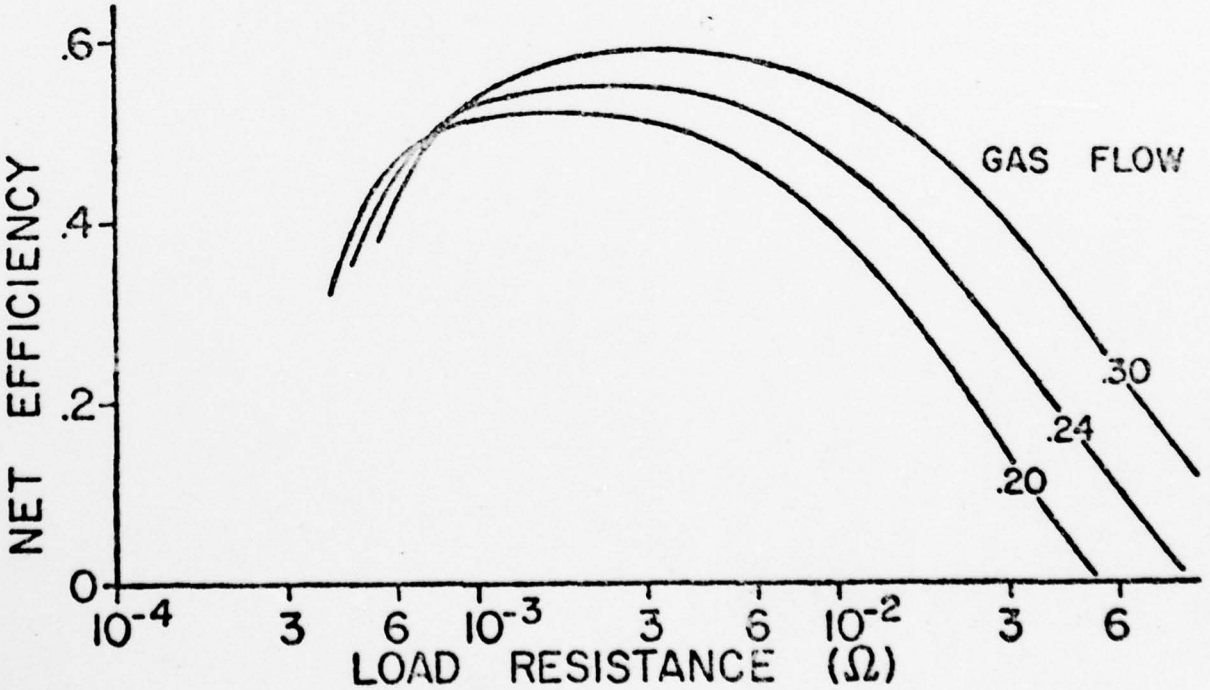

Figure 3.5- Generator net efficiency under identical conditions as illustrated in Figure 3.4.

Note that the gross efficiency curve for gas flow rate 0.2 kg/s would be multiplied by a smaller constant than the curve for gas flow rate 0.3 kg/s, reflecting the smaller void fraction and relatively larger pump work of the 0.2 kg/s case. Note, too, that for heavier loads, the net efficiency drops to less than forty five percent. This neglects those loss mechanisms accounting for the discrepencies between real and inviscid model gross efficiencies, and it assumes that the liquid metal can be pumped with no losses. Net efficiency of a real generator will be accordingly lower.

Figures 3.6 through 3.8 portray channelwise variations in some flow parameters for a gas flow rate of 0.3 kg/s. These results are typical of flows under most condition. In Figure 3.6, note an increase in pressure gradient with decreasing load resistance. Decreasing the load,decreases the electric field and so increases the magnitude of the Lorentz force. For a load resistance of 0.00041 ohm the drop in pressure is sufficient to expand the mixture to a very large void fraction, Figure 3.7. The result is a large liquid velocity and a large pressure drop near the channel exit. Slip for this case, Figure 3.8, also rises sharply near the exit, as should be expected for a large void fraction, large pressure gradient flow. For a load of 0.0044 ohm, the liquid velocity drops enough that the pressure gradient reverses near the exit (Figure 3.6). The slip over this region of the channel drops below unity.

Figures 3.9 through 3.14 represent channel operation at a liquid flow rate of 8.0 kg/s, an inlet pressure of $10^6 N/m^2$, and a uniform magnetic flux density of 0.3 Tesla. Nitrogen flow ranges from 0.2 kg/s to 0.45 kg/s.

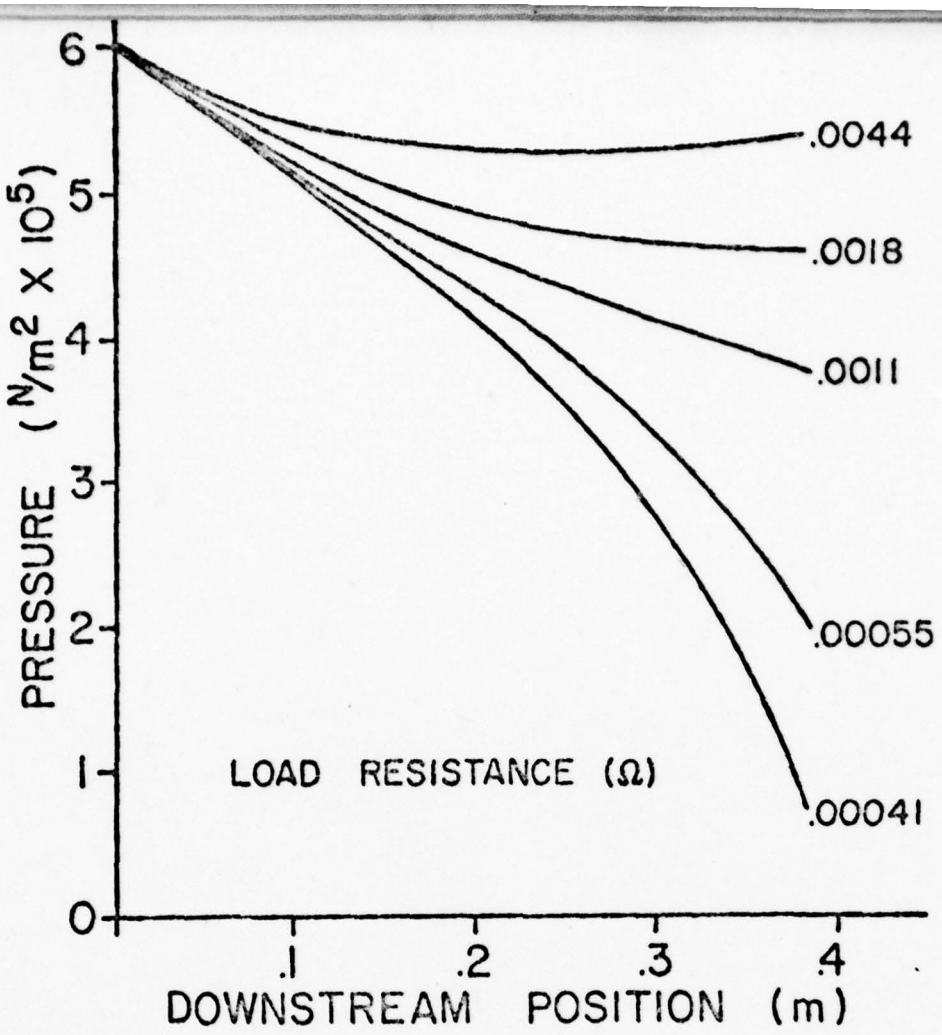

Figure 3.6- Pressure versus downstream position in generator channel. Gas flow rate 0.3 kg/s; liquid flow rate 15 kg/s; flux density 1.2 T; and inlet pressure 6.10^5 N/m^2, under various load resistances.

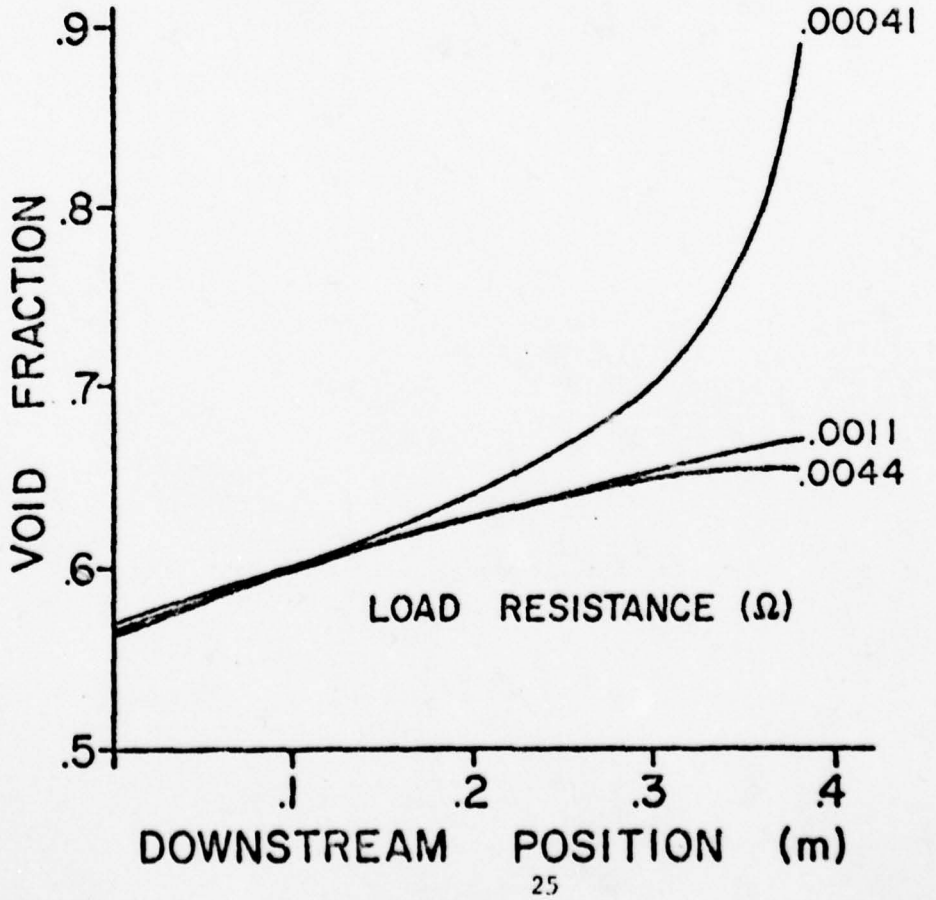

Figure 3.7- Void fraction versus downstream position in generator channel. Same data as shown in Figure 3.6.

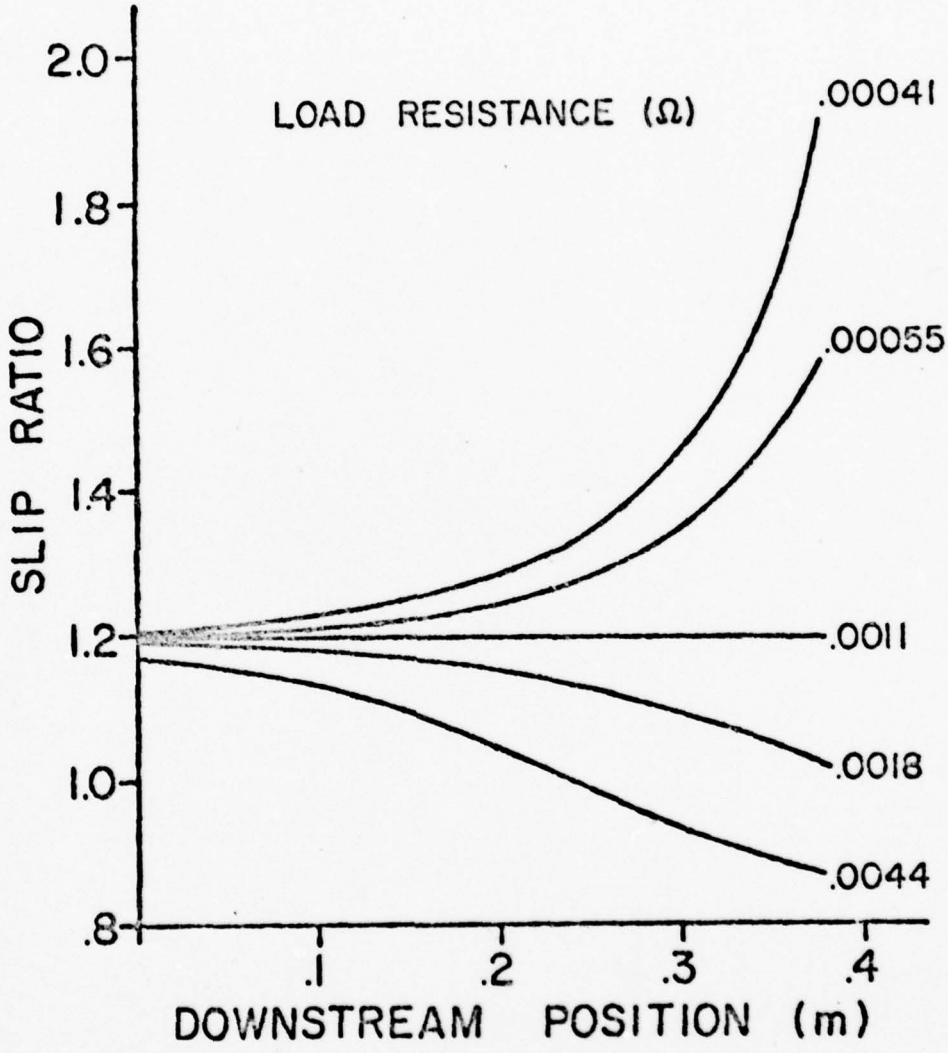

Figure 3.8- Slip ratio versus downstream position in generator channel. Gas flow rate 0.3 kg/s; liquid flow rate 15 kg/s; flux density 1.2 T; and inlet pressure 6.10^5 N/m^2, under various load resistances.

Figure 3.9 shows the variation of load voltage as a function of load resistance. Generally, as the load resistance increases, the voltage approaches some constant value. This behavior is typical of Faraday generators (Hughes and Young, 1966).

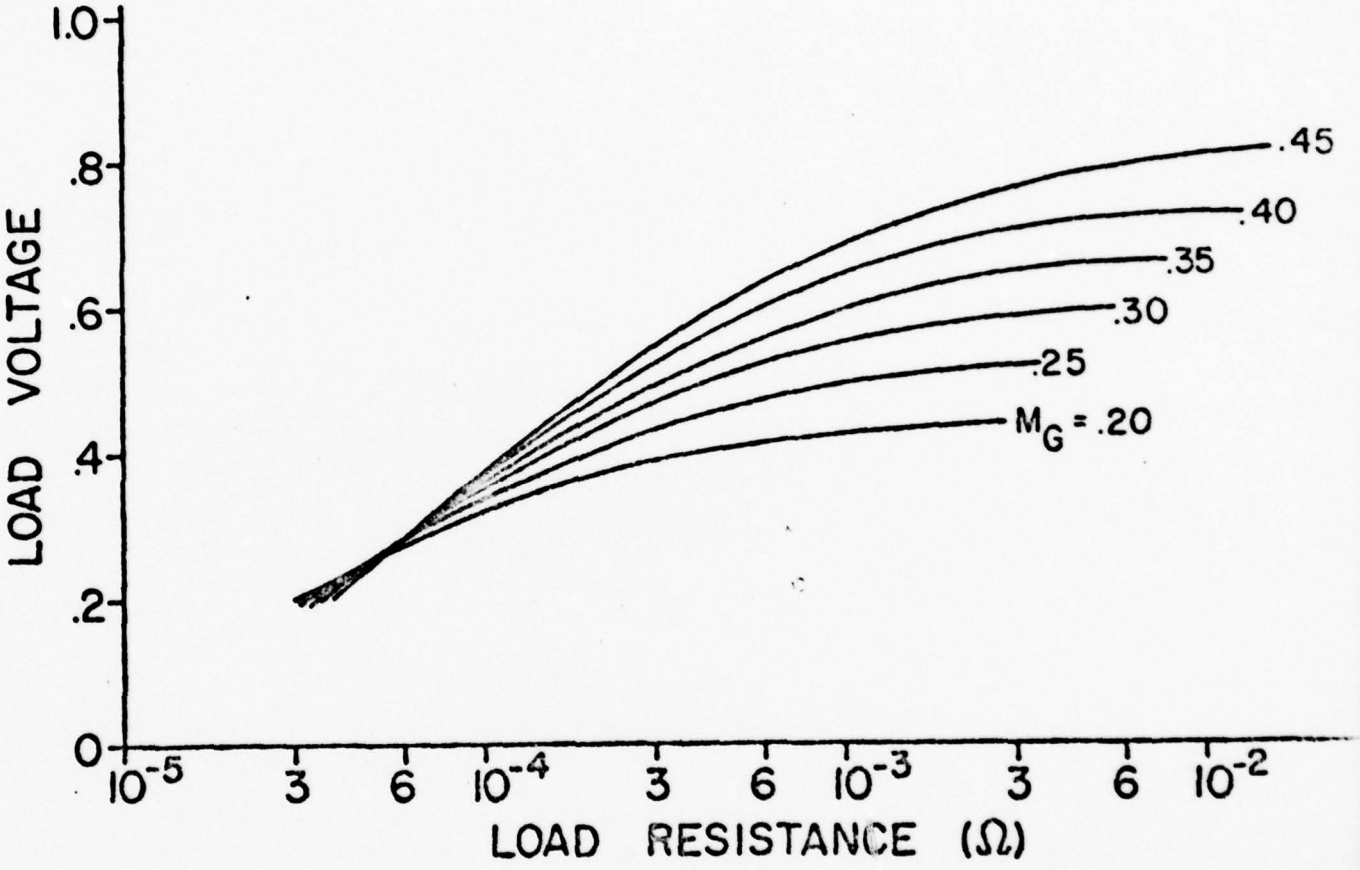

Figure 3.9- Load voltage versus load resistance for liquid flow rate 8 kg/s; flux density 0.3 T; and inlet pressure 10^6 N/m^2. M_G is Nitrogen mass rate flow in kg/s.

In Figure 3.10 the net power has been plotted versus load voltage. As might be expected, more net power is available with high gas flow rates. But for small load voltages, no advantage can be

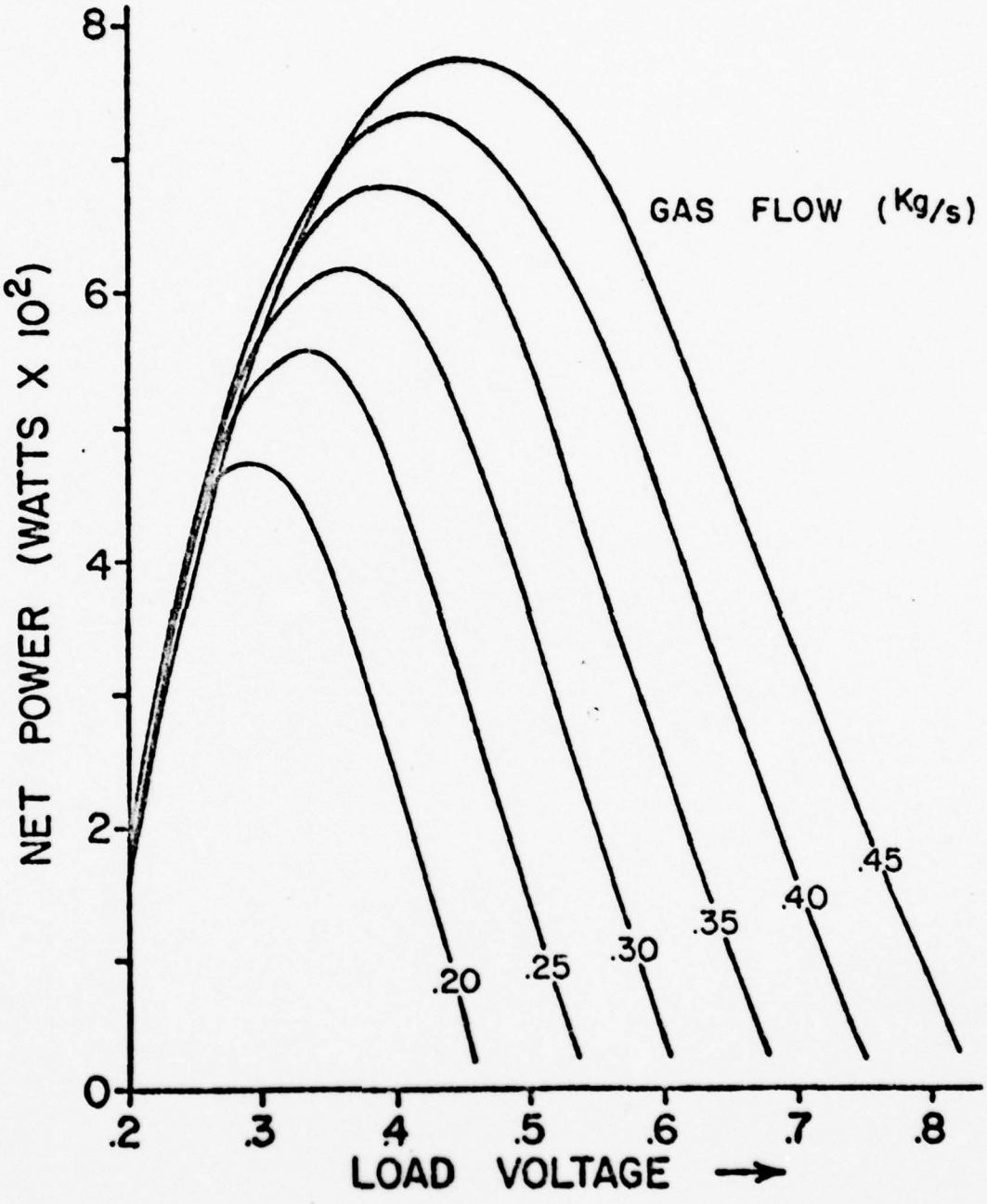

Figure 3.10- Net power versus load voltage for the flow conditions documented in Figure 3.9.

gained by increasing the gas flow. This occurs as a result of the large pressure gradients of small load voltages leading to large slippage losses for large gas flows. Figure 3.11 shows the loss in efficiency caused by this effect.

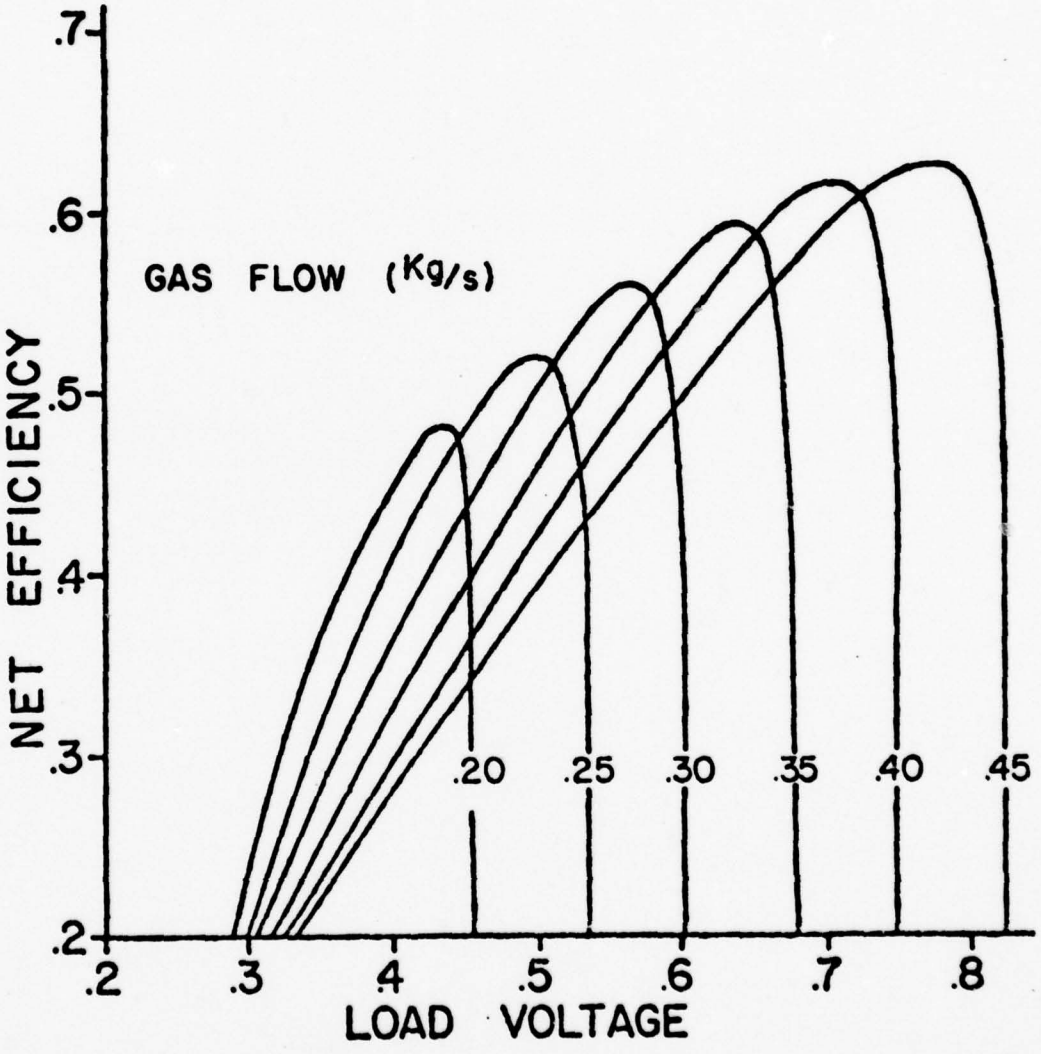

Figure 3.11- Net efficiency versus load voltage for the same generator, under the same flow conditions as previously, i.e. liquid flow rate 8.0 kg/s; flux density 0.3 T; and inlet pressure 10^6 N/m^2.

Figure 3.12 shows how the power required to pump the NaK increases with decreasing load voltage. The pump power increases with the flow rate of Nitrogen. This is so because the net power of the generator exhibits increasing optima for increased load voltage and gas flow rate by certain ratios. This tendency breaks down at load voltages below $\sim$ 0.3V as indicated in the diagrams of Figure 3.12 where the curves intersect each other.

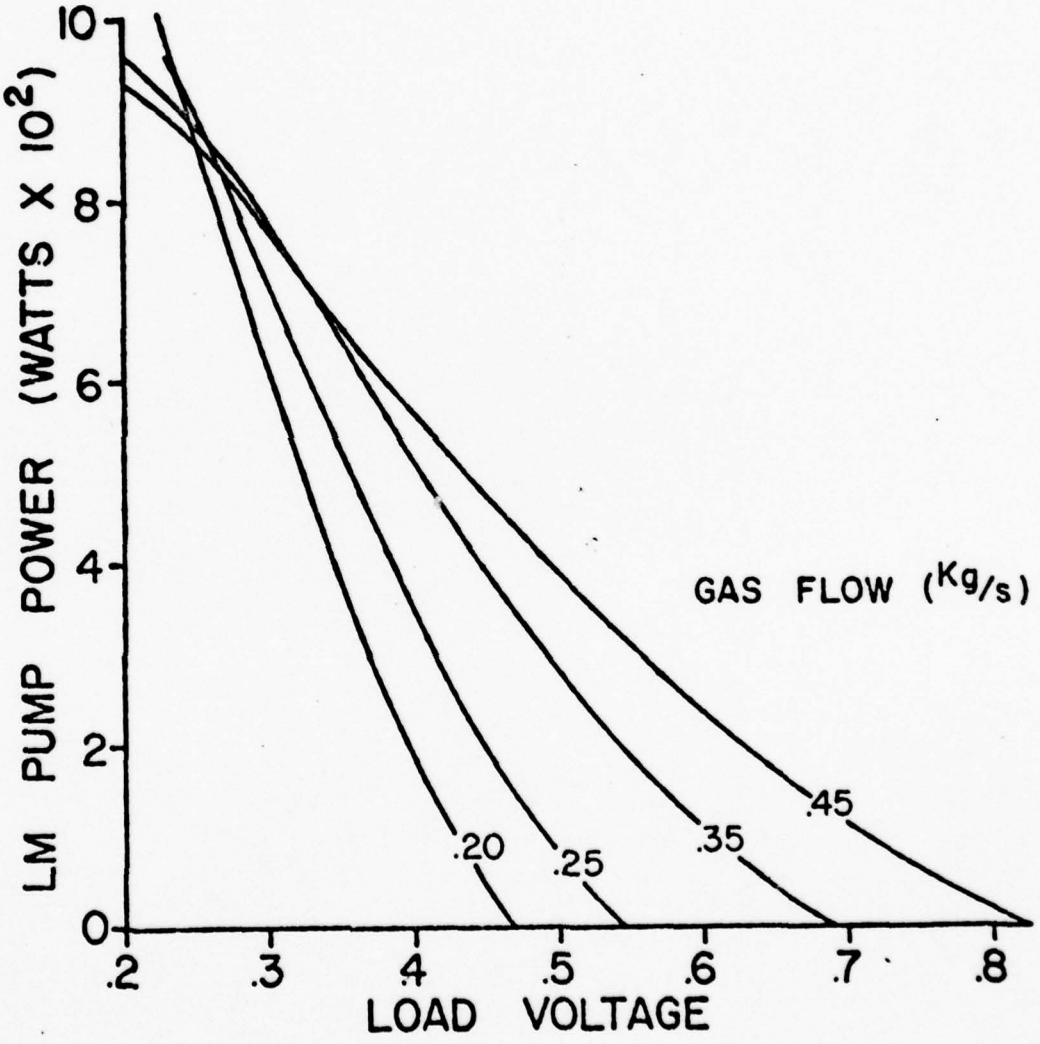

Figure 3.12- Liquid metal pump power versus load voltage at a NaK flow rate of 8.0 kg/s; flux density 0.3 T; and inlet pressure 10^6 N/m^2.

Figures 3.13 and 3.14 illustrate streamwise dependence of gas and liquid velocities and of electric current density for different load voltages.

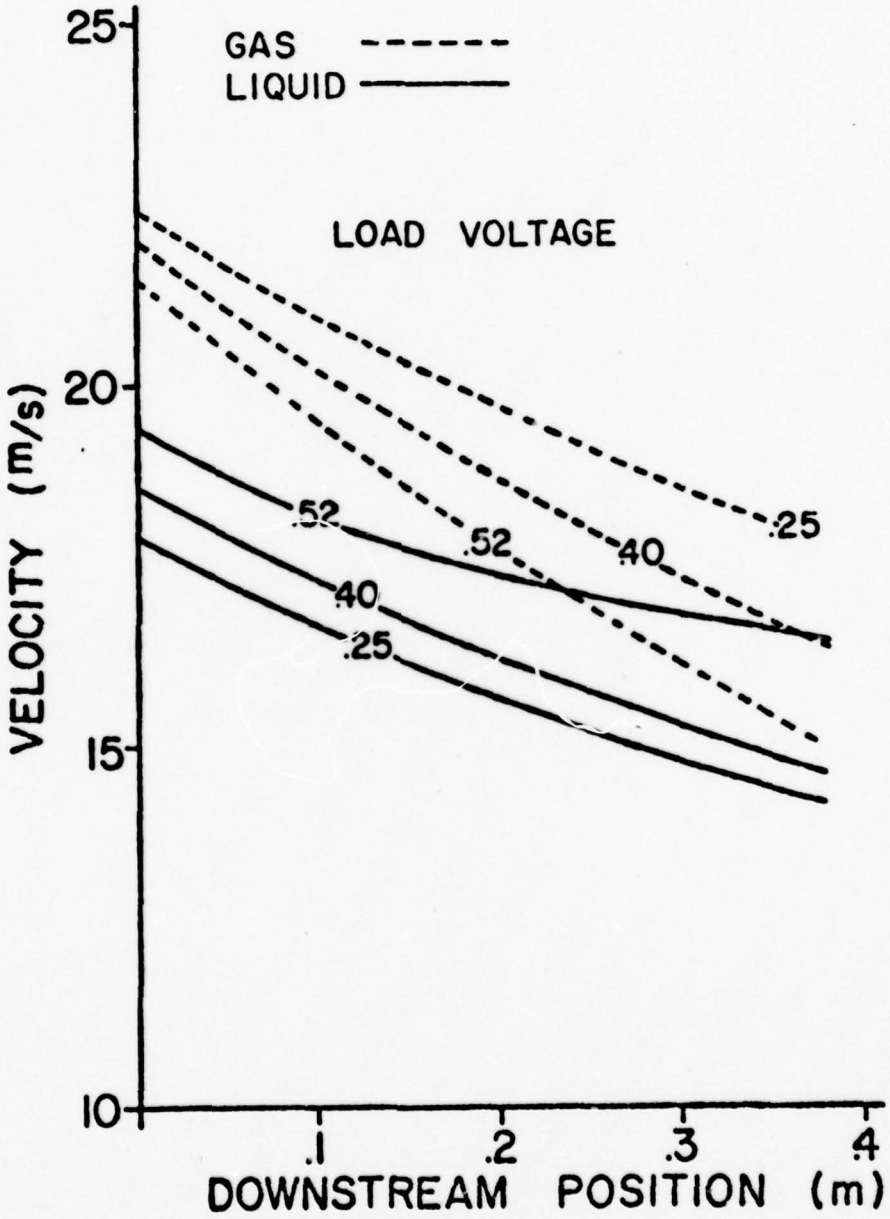

Figure 3.13- Fluid velocity versus downstream distance in the generator duct for gas flow rate 0.35 kg/s; liquid flow rate 8.0 kg/s; flux density 0.3 T; and inlet pressure 10^6 N/m^2.

Since efficient operation of Faraday generators (at large Hartmann number) requires that the applied electric field E be nearly equal in magnitude to the induced electric field $u_L B$ (see equation (3.6)), small variations in u_L can lead to relatively large variations in current density. This effect is evident in Figures 3.13 and 3.14. The curves for a load voltage of 0.52 is interesting from a physical standpoint: note that there is a sign change of the pressure gradient where the current density changes sign and that, at the same place, the gas and liquid velocities are equal. (Compare Figure 3.13.)

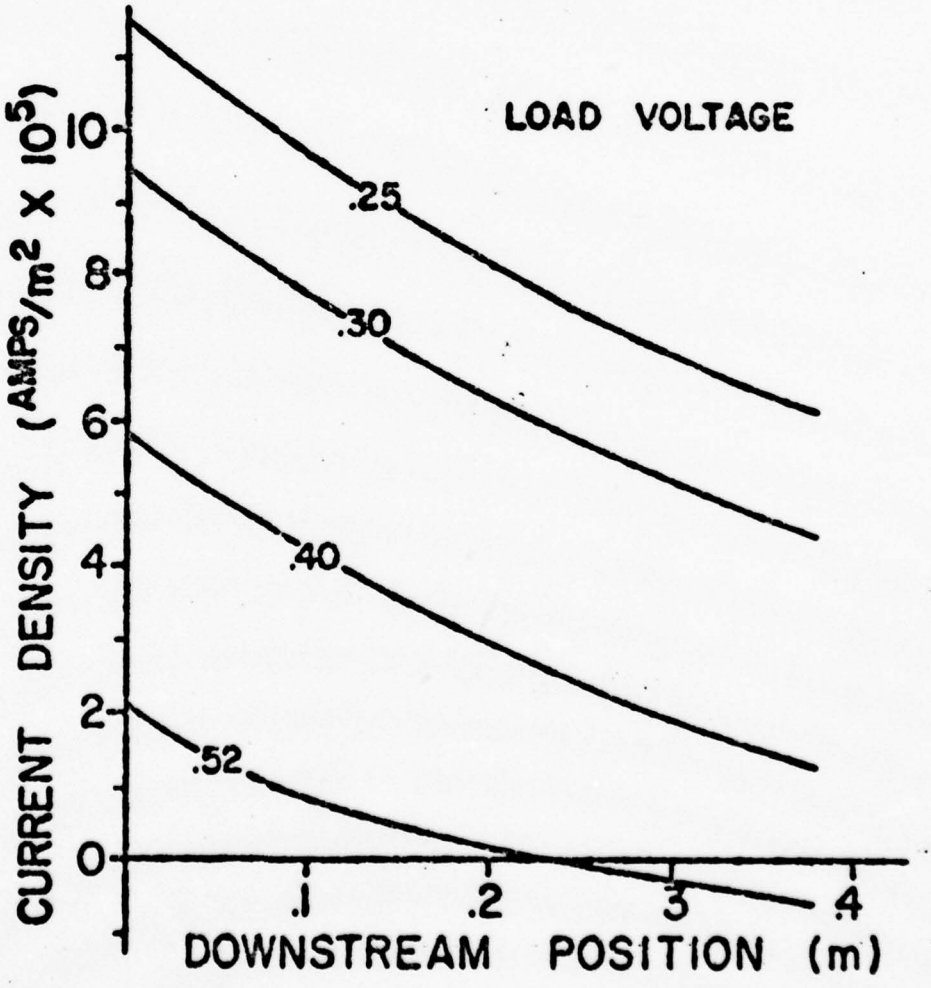

Figure 3.14- Electric current density versus downstream distance in the generator duct. The same flow conditions as documented in Figure 3.13.

Figures 3.15 through 3.17 illustrate the effects of variation of applied flux density for fixed inlet pressure and fluid flow rates. It can be seen from Figure 3.15 that an increase in flux density at a fixed load resistance results in a higher net power level.

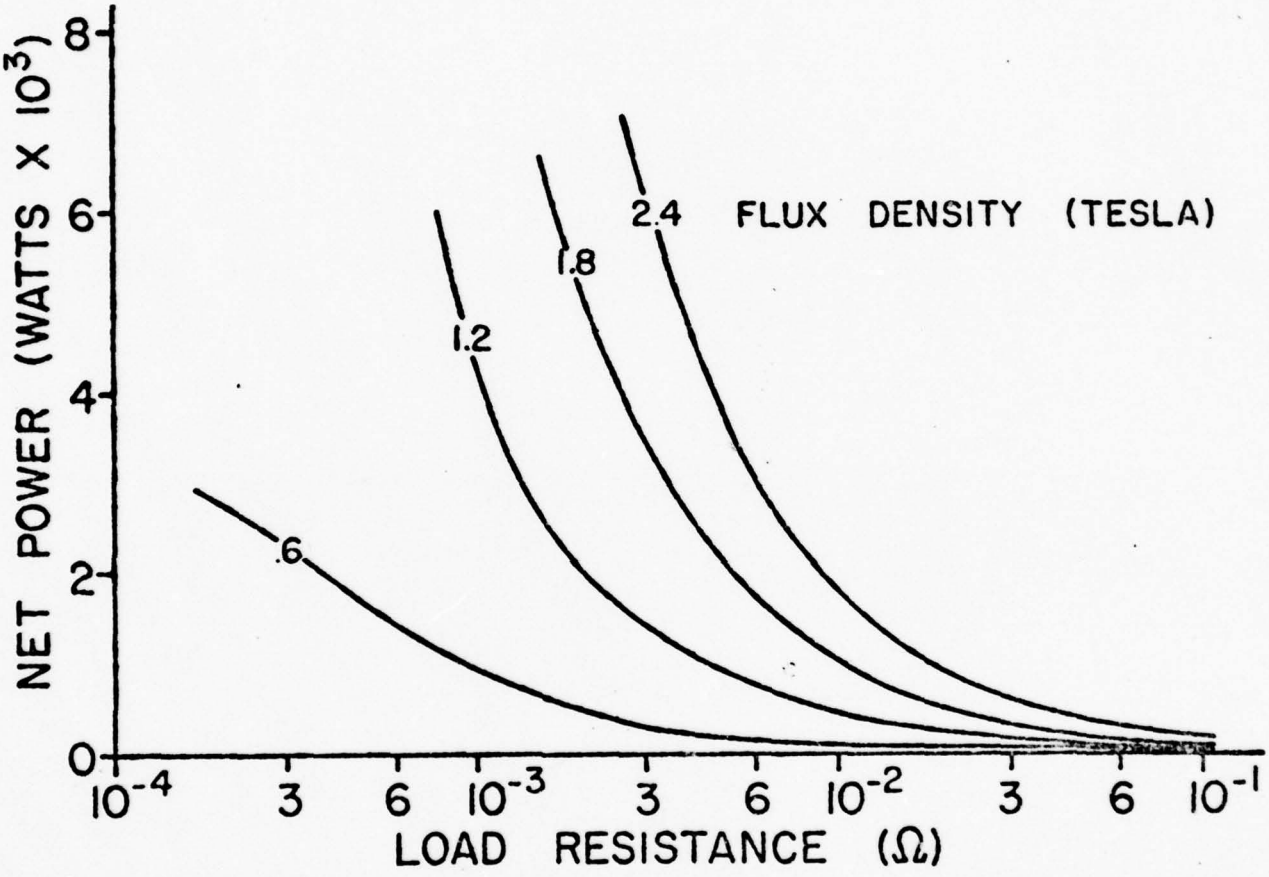

Figure 3.15- Net power versus load resistance for gas flow rate 0.1 kg/s; liquid flow rate 8.0 kg/s; inlet pressure 3.10^5 N/m^2; and various flux densities 0.6 - 2.4 T.

Changes in flux density affect the efficiency, Figures 3.16 and 3.17, much as did changes in gas flow rate in the previous examples. For a given flux density, there is an optimum load, and for a given load there is an optimum flux density.

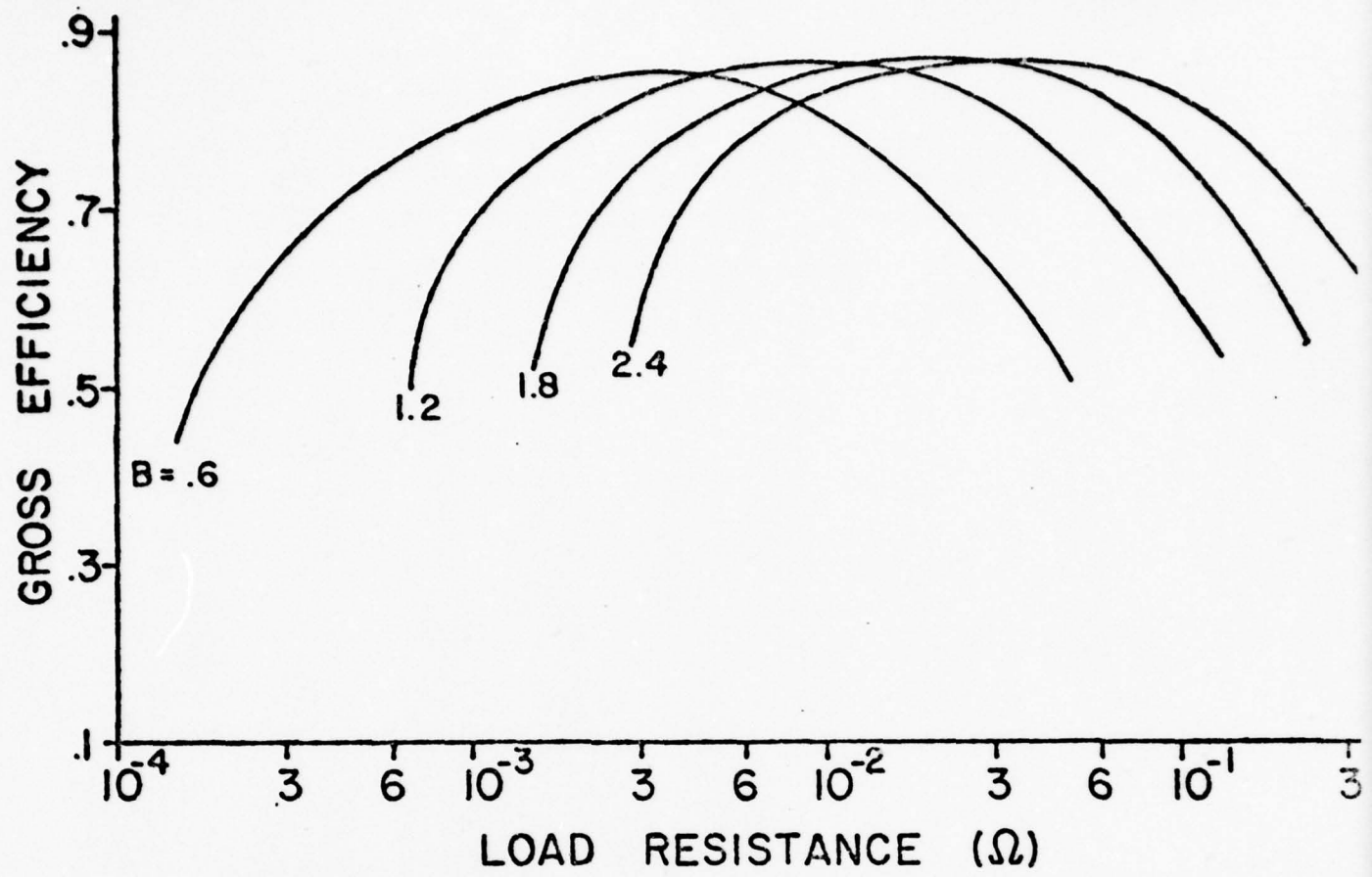

Figure 3.16- Gross efficiency versus load resistance for gas flow rate 0.1 kg/s; liquid flow rate 8.0 kg/s; inlet pressure 3.10^5 N/m^2; under various flux densities, B (in Tesla).

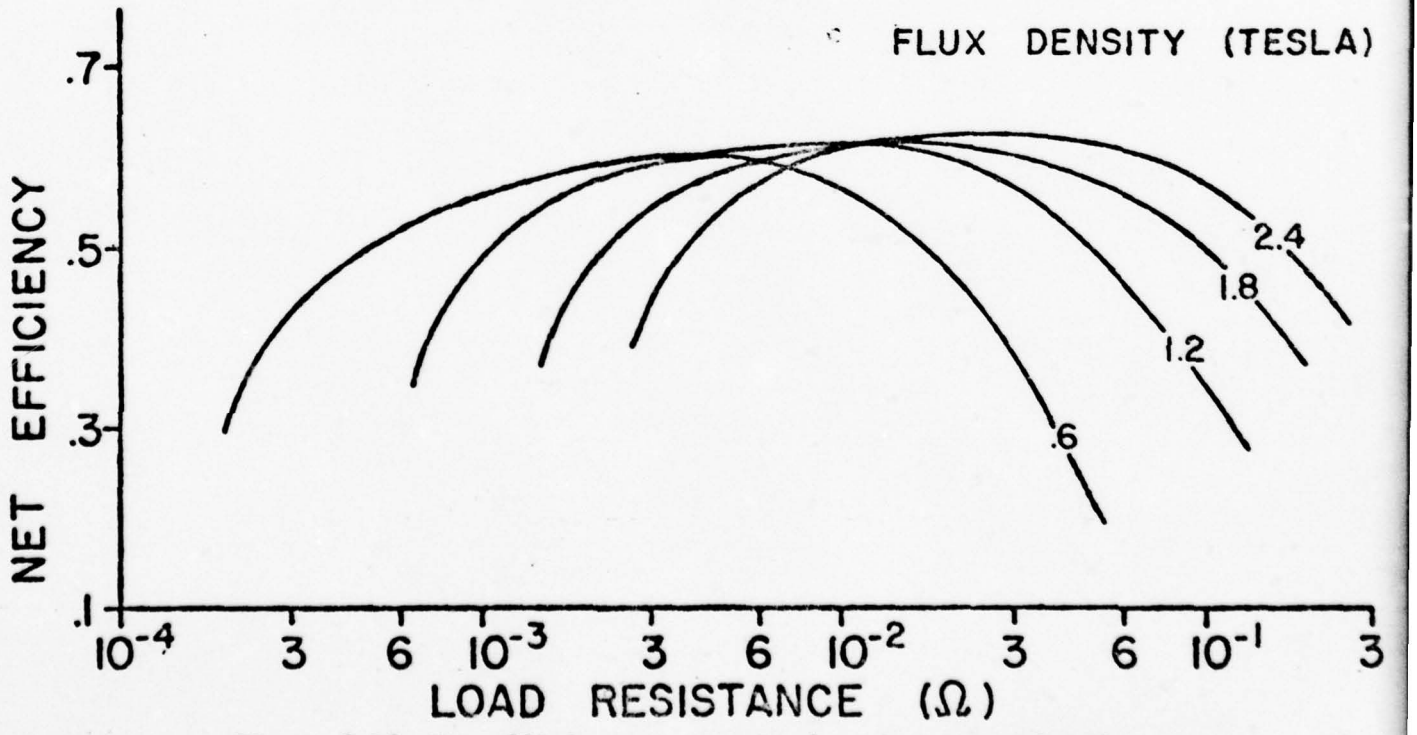

Figure 3.17- Net efficiency versus Load resistance under the same generator conditions as in Figure 3.16.

In summary, the model generator, considered here, has a maximum gross efficiency for all cases examined of around ninety percent and a maximum net efficiency of around sixty percent. These maxima occur at very low power levels corresponding to small pressure gradients. The physical interpretation for this is that slip losses are least at small pressure gradients. Efficiency tends to be higher, too, when the liquid velocity is nearly constant throughout the channel. In that case, the channel operates under uniform loading conditions.

However, the losses of a real generator can exceed the low power output of the most efficient inviscid generator described in the last paragraph. Consequently, a real generator is most efficient under heavier loads, loads which correspond in the inviscid model to a gross efficiency of around seventy percent and a net efficiency of around forty percent. This neglects viscous losses and losses due to three dimensional effects and end effects. The experimental generators at Argonne National Laboratory have a maximum gross efficiency of around sixty percent. The maximum net efficiency is, therefore, around thirty percent. Additional friction losses will be incurred in pumping the liquid and gas. Note that these efficiencies describe losses inherent in the turbine/generator mechanics and do not include the thermodynamic efficiency of the gas cycle.

Pressure distributions and power outputs predicted by the presented model reflect many features of the experiments carried out at Argonne National Laboratory. The model fails at large load resistances, but that was anticipated and, in any case, is outside the region of interest for practical power generation. More importantly, the model does appear to represent a valid upper limit on the efficiency and power output of the real generator.

On the other hand, the predictions by the model of void fraction, velocity and slip do not generally agree with the experimental data. This is cause for concern, since these parameters are important in component design (see the discussion of constant velocity generators in Chapter 5, for example). There is evidence of a source of error in the gamma ray attenuation technique used at Argonne National Laboratory to measure void fraction and to infer velocity and slip. Analysis of such a system by Hooker and Popper (1958) indicates that void distribution must be taken into account when the gamma ray attenuation technique is used. The reported measurements are based on an assumption of uniformly distributed voids, while in fact there is probably a large degree of slugging present (see Wallis, 1969 for a description of churn turbulent flow). As a result, the published void fractions could be as much as twenty or thirty percent too large.

Equations (3.7) and (3.8) can be used to estimate the error in slip arising from an error in measured void fraction. We have for the slip S

$$S = \frac{u_G}{u_L} = \frac{q_G}{Pk\alpha} \quad \frac{\rho_L(1-\alpha)}{q_L} \tag{3.14}$$

Differentiate with respect to α to get

$$\frac{\partial S}{\partial \alpha} = - \frac{q_G \rho_L}{q_L P k} \alpha^{-2} \tag{3.15}$$

From equations (3.7) and (3.8) we have

$$\frac{q_G \rho_L}{q_L P k} = \frac{\alpha S}{1-\alpha} \tag{3.16}$$

so that equation (3.15) becomes

$$\frac{\partial S}{\partial \alpha} = - \frac{S}{\alpha(1-\alpha)} \tag{3.17}$$

Equation (3.17) gives a formula for estimating the relative error in the slip $\frac{\Delta S}{S}$

$$\frac{\Delta S}{S} \approx - \frac{\Delta \alpha}{\alpha(1-\alpha)} \tag{3.18}$$

This formula indicates that the slip reported for the experiments at Argonne National Laboratory may be as much as fifty percent in error. Such an error may explain some of the anomolous slip behavior documented in ANL reports, where slips less than unity have frequently been noted for large upstream pressure gradients (see, for example, Petrick et al, 1978).

In the same fashion, the experimental reports probably overestimate the average velocity of the liquid phase. Although the relative error of the reported velocity would not be so large as that of the slip, the effect of that error could be large. This is true since, at large load factors, the Lorentz force is very sensitive to velocity changes.

Chapter 4

ONE DIMENSIONAL MODEL OF A COMPENSATING SYSTEM OF A FARADAY GENERATOR

Up to this point, the magnetic flux has been assumed to be uniform as applied. This is equivalent to assuming that every point in the channel is perfectly compensated, and is a necessary condition for optimum efficiency of generators being reported here (Jackson, 1963).

Electric current in the LT-3 generator at Argonne National Laboratory is returned in the external circuit through uniform compensating bars above and below the channel (see Figure 3.1). Since the current is not produced uniformly along the channel length and since the compensating bars are some distance removed from the channel. The system is not perfectly compensated. In order to evaluate the effects of imperfect compensation, we have developed an averaged Ampere's law suitable for use with our one dimensional model. Ampere's law can be written (Holt and Haskell, 1965):

$$B_y(x,y,z) = -\frac{\mu_e}{4\pi}\int_{-\infty}^{\infty}\iint\left(\frac{x'-x}{r^3}\right) J_{z'}\, dx'\, dy'\, dz' \qquad (4.1)$$

where $x=x_1$, $y=x_2$, $z=x_3$ as shown in Figure 2.1. B_y is the component of the flux density in the direction of the applied flux density, μ_e is the permeability of free space, and J is the current density. The integration takes place over the entire electrical circuit.

To reduce equation (4.1) to a one dimensional form, we average over y and z

$$\overline{B}_y(x) = -\frac{\mu_e}{16\pi wh(x)}\int_{x'}\int_{y'}\int_{z'}\iint_{x}\iint_{y}\left(\frac{x'-x}{r^3}\right) J_{z'}\, dx'dy'dz'dydz \qquad (4.2)$$

where w=b is the half width between electrodes and h (x)=a, is the half channel height (see equation 3.11).

It is convenient to write equation (4.2) as

$$\bar{B}_y(x) = -\frac{\mu_e}{4\pi} \int_{x'} K(x',x)\, J_z,(x')\, dx' \qquad (4.3)$$

where

$$K(x',x) = \frac{(x'-x)}{4wh(x)} \int_{y'}\int_{y}\int_{z'}\int_{z} \frac{1}{r^3}\, dy'dz'dydz \qquad (4.4)$$

with

$$r = \left((x-x\ )^2 + (y-y\ )^2 + (z+z\ )^2\right)^{\frac{1}{2}} \qquad (4.5)$$

The integration in equation (4.4) over y, y', and z', although cumbersome, is straightforward.

$$K(x',x) = \frac{1}{hw}\int_{-w}^{w}\left[\tan^{-1}\left(\frac{(w-z)(h'+h)}{(x'-x)(x-z)^2 + (x'-x)^2 + 4h^2)^{\frac{1}{2}}}\right)+\right.$$

$$\left.\left(\frac{x'-x}{h}\right)\ \ell n\left(\frac{((w-z)^2 + (x'-x)^2 + 4h^2)^{\frac{1}{2}} + (w-z)}{((w-z)^2 + (x'-x)^2)^{\frac{1}{2}} + (w-z)}\right)\right] dz$$

Final integration over z we have done numerically. Note that K(x',x) need be determined only once for a given channel and compensating system. Thereafter, it can be used to evaluate $\bar{B}$ for any current distribution in that channel. The numerical values of K(x',x) are listed in Appendix 2.

In our analysis, we considered only the current flowing through the channel and through the compensating bars as contributing to the induced magnetic field. Under those conditions, we find

$$\bar{B}\ (\xi) = B_o\ (1 + \frac{R_M}{4\pi}) \int_{o}^{\xi}\left[\frac{1}{d}F(\xi)h(\xi')-K(\xi,\xi')\right]\left[E + u\bar{B}(\xi')\right]\ d_{\xi}' \qquad (4.6)$$

where B_o is the (average) applied magnetic field,

and d is the compensating bar thickness. R_M is the magnetic Reynolds number

$$R_M = u_o \ell \sigma_L \mu_e \tag{4.7}$$

with u_o the average velocity in the x-direction while,

$$\xi = \frac{x}{\ell} \tag{4.8}$$

and

$$F(\xi) = \int_o^1 K(\xi', \xi)\, d\xi' \tag{4.9}$$

For a given set of generator operating parameters, equation (4.6) can be solved iteratively to determine flow conditions. We start by the input of a constant flux density and calculating the resultant current distribution. A corrected flux density is then calculated via equation (4.6), and the process repeated until satisfactorily converged. In most cases, we found three or four iterations were sufficient. Table 4.1 decuments the computer results for the compensated channel. The results are typical in that the compensation of the LT-3 generator at Argonne National Laboratory is quite good. Note that, in spite of the fact that current density varies by a factor of twenty, over the length of the channel, the magnetic flux density varies by less than one tenth of one percent. In none of the cases we examined did the magnetic flux density vary by as much as one percent over the length of the channel. Except at very low power levels, efficiencies for the most extreme cases were never less than ninety eight percent of those for perfectly compensated cases. It is clear from these computer tests that one need not include a magnet model in the description of the LT-3

Position (m)	Pressure (N/m^2)	Void fraction	Current density (Amp/m^2)	Actual flux (B/B_o)
0	$10 \cdot 10^5$	.656	$6.14 \cdot 10^5$	.9965
.077	$9.52 \cdot 10^5$	.672	$4.09 \cdot 10^5$	1.0006
.154	$9.15 \cdot 10^5$	.689	$2.32 \cdot 10^5$	1.0007
.231	$9.00 \cdot 10^5$	.700	$1.44 \cdot 10^5$	1.0006
.308	$8.89 \cdot 10^5$	.713	$0.678 \cdot 10^5$	1.0002
.385	$8.85 \cdot 10^5$	.727	$0.390 \cdot 10^5$	1.0000

Table 4.1 Effects of imperfect compensation in the two-phase LT-3 generator at Argonne National Laboratory. NaK flow rate 8.0 kg/s; N_2 flow rate 0.3 kg/s; terminal voltage 2.1V; applied flux density (B_o) 1.2 T; load resistance 1.42 mΩ.

generator at Argonne. Assumption of a uniform applied flux density is a minor source of error.

Chapter 5

ONE DIMENSIONAL MODEL OF A ZERO SLIP TWO PHASE FARADAY GENERATOR

An ideal two phase Faraday generator would operate with no slip between the gas and liquid phases. How such a flow might be attained is not clear, but elimination of slip constitutes elimination of an important loss mechanism. It is useful to study a zero slip model, since by comparing it to a model with slip, one can get a handle on the energy cost of the slip.

As before, we neglect the contributions of viscosity and inertia to the downstream pressure gradient and assume perfect compensation and no end losses. The governing equations for a one dimensional, zero slip model are then

$$q_L = A(1-\alpha)\, u_L \rho_L \tag{3.8}$$

$$q_G = A\alpha u_G P k \tag{3.7}$$

$$\frac{\partial P}{\partial x} = -\sigma B(E + u_L B) \tag{3.6}$$

$$\sigma = \sigma_L\, f(1-\alpha) \tag{3.9}$$

Note that the velocity,

$$u = u_L = u_G \tag{5.1}$$

is the same for both phases. As in Chapter 3, $f(1-\alpha)$ is a semiempirical function relating liquid fraction and liquid conductivity to dispersed liquid conductivity.

These assumptions lead again to a model that is easy and efficient to examine interactively with a computer, and which preserves the major force and energy mechanisms of a zero slip system.

Figures 5.1 through 5.4 illustrate the operation of a zero slip generator with an applied flux density of 1.2 T, a gas flow rate of 0.1 kg/s, a liquid flow rate of 8.0 kg/s, and an inlet pressure of 3.10^5 N/m^2. These are the same operating conditions as for one of the examples in Chapter 3.

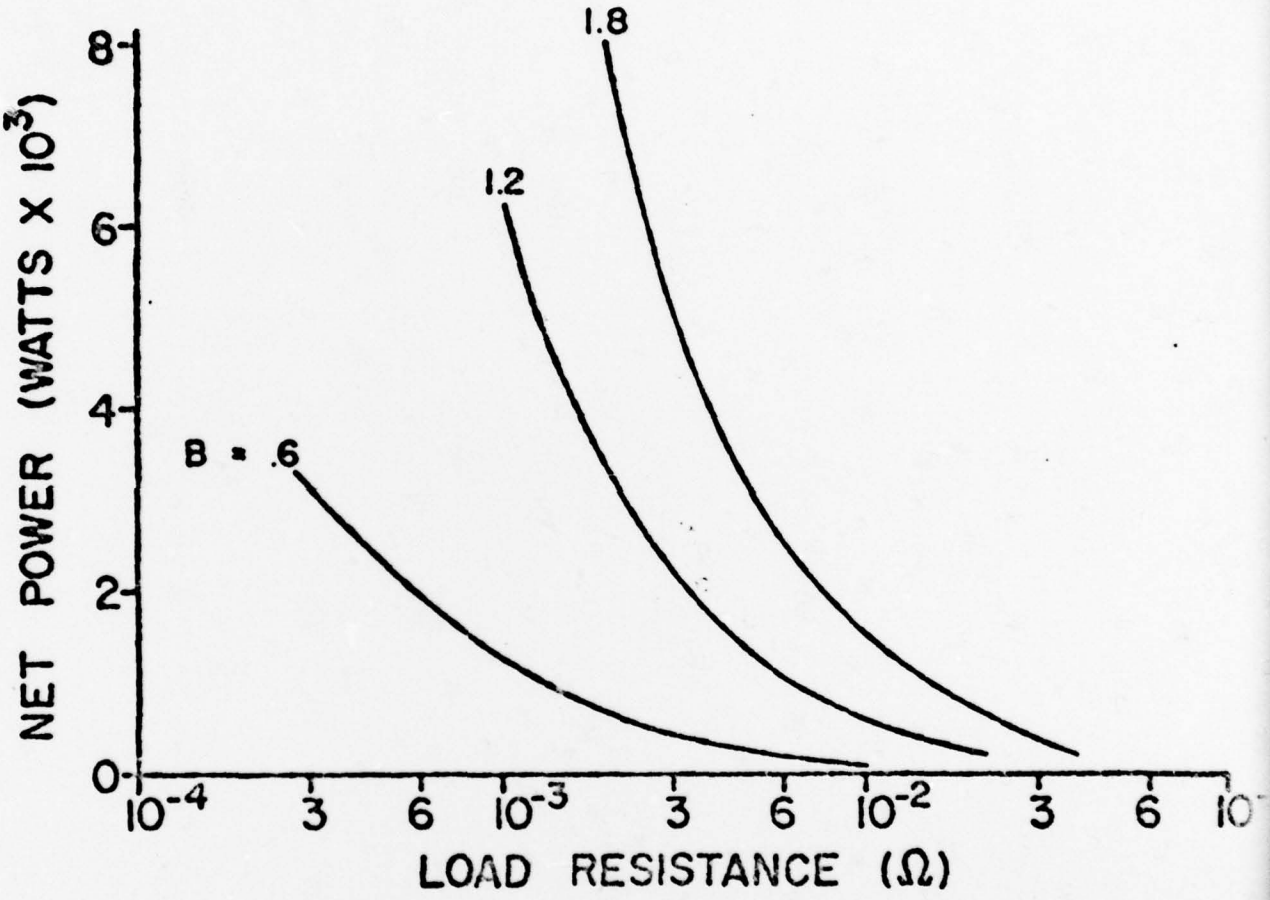

Figure 5.1- Net power versus load resistance for a zero slip generator, corresponding to the LT-3 generator at Argonne National Laboratory operating under the same conditions as illustrated by Figure 3.15; gas flow rate 0.1 kg/s; liquid flow rate 8.0 kg/s; inlet pressure 3.10^5 N/m^2. Various flux densities B (in Tesla).

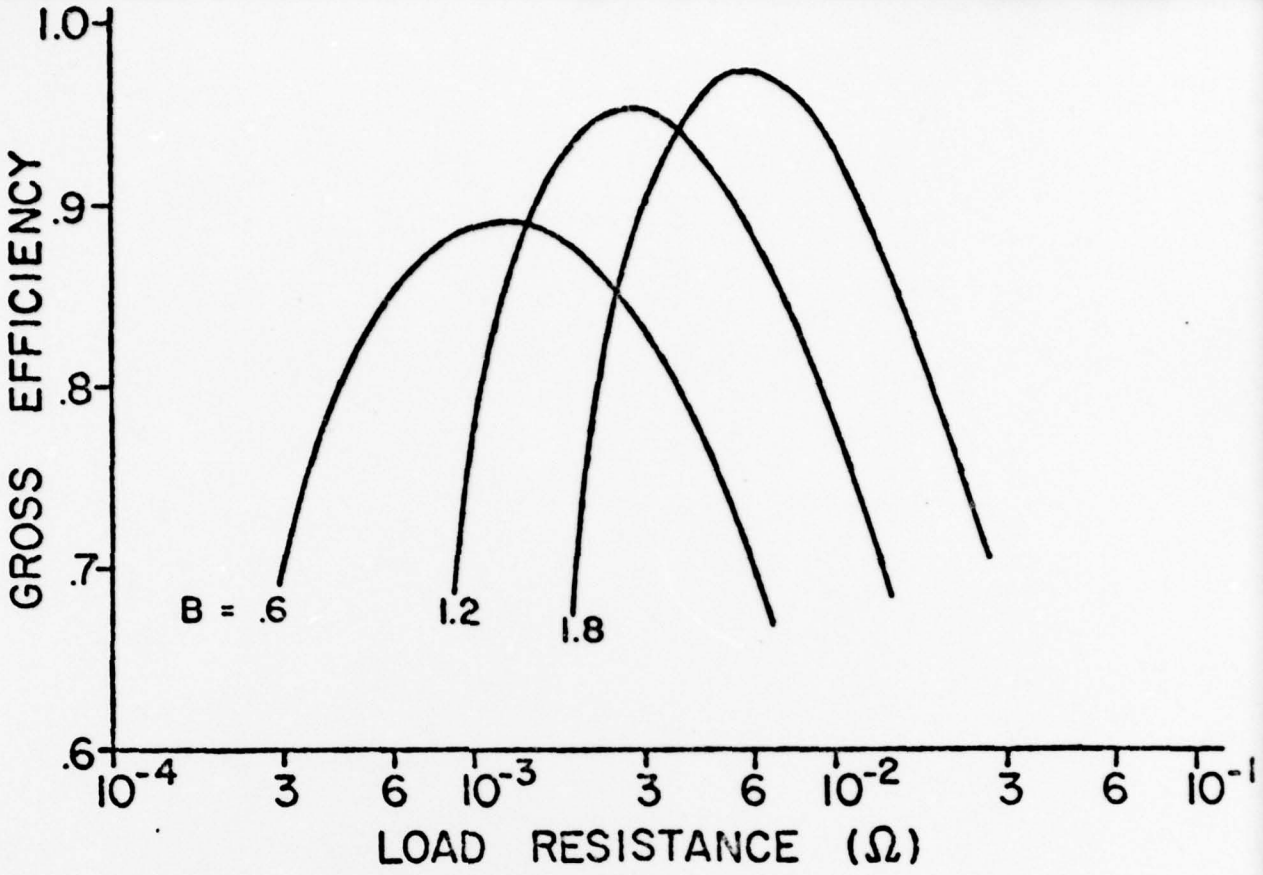

Figure 5.2- Gross efficiency versus load resistance for the zero slip generator at a gas flow rate 0.1 kg/s; liquid flow rate 8.0 kg/s; inlet pressure $3.10^5 N/m^2$; under various flux densities B (in Tesla).

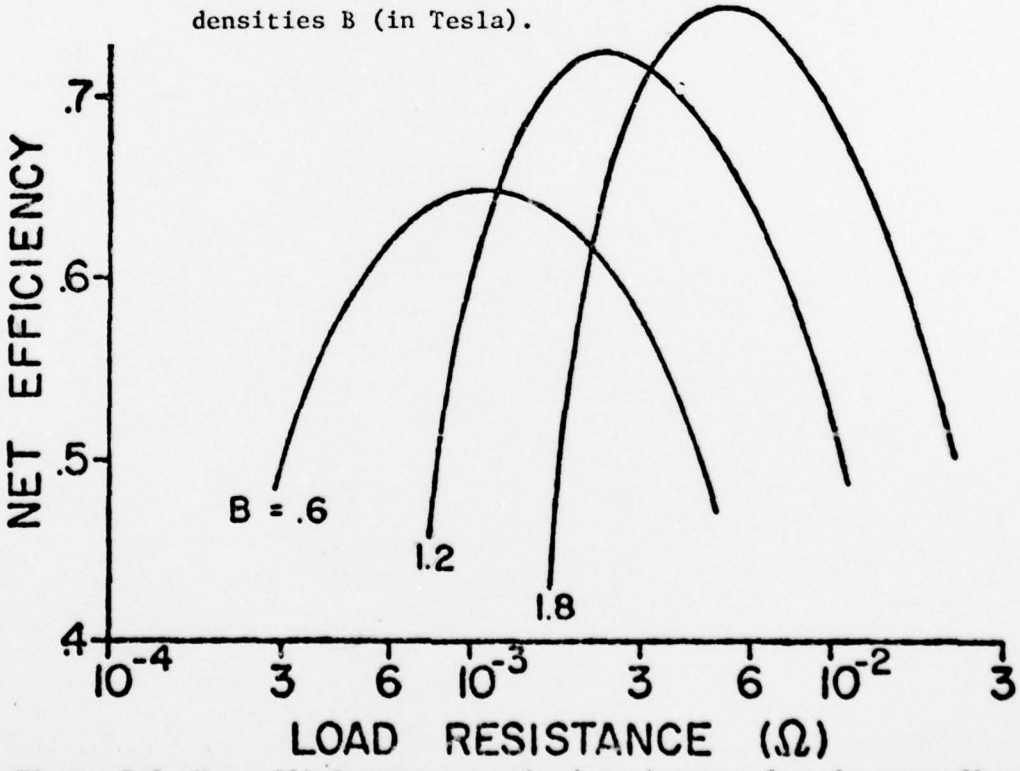

Figure 5.3- Net efficiency versus load resistance for the same flow cases illustrated in Figure 5.2.

The major difference between the case with slip and the case without is that the efficiency and power level are both higher without slip. Note in Figure 5.2 that the gross efficiency can approach unity. This occurs when the liquid passes through the generator at near constant velocity. The peak gross efficiency for the no slip case occurs at a smaller load resistance and is more sharply demarked than for the slip case (compare to Figure 3.16). The difference can be attributed to the fact that slip losses, when they occur, are larger for smaller load

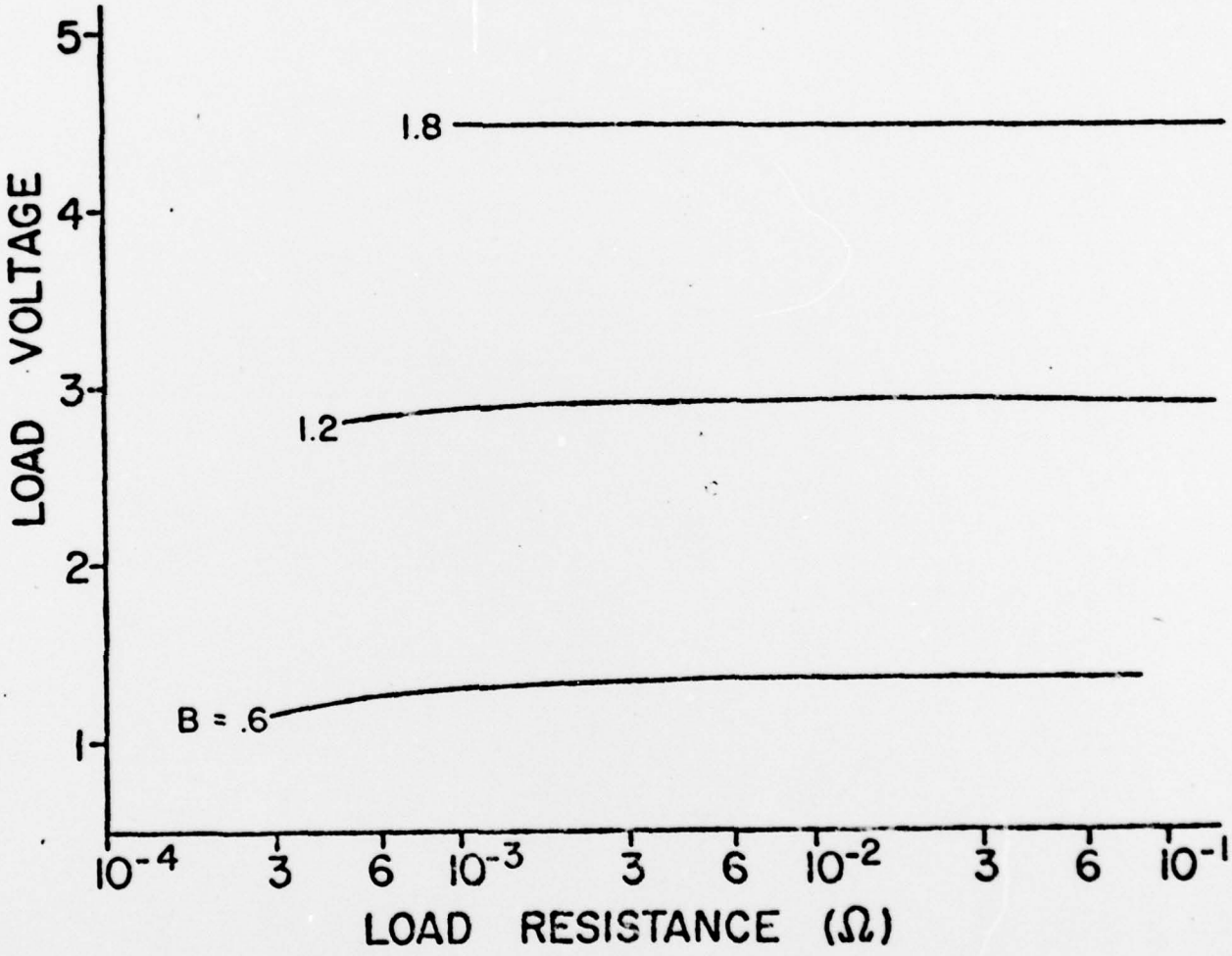

Figure 5.4- Load voltage versus load resistance for the no slip generator at a N_2 flow rate 0.1 kg/s; NaK flow rate 8.0 kg/s; and inlet pressure 3.10^5 N/m^2 under various flux densities B (in Tesla). These are the same flow cases as specified in Figures 5.1 - 5.3.

resistances. The net efficiencies with slip (Figure 3.17) and with no slip (Figure 5.3) differ in much the same manner as do the gross efficiencies. As a result of better coupling and better efficiency, power levels are higher without slip (Figure 5.1) for a given load or a given efficiency (compare to Figure 3.15). Figure 5.4 plots load voltage versus load resistance. Note that the voltage is nearly constant for this case over the entire range of interesting loads.

If viscosity is neglected, Joule losses are smallest when the electrically conducting liquid moves at the same velocity everywhere. This can be shown through variational principles (Medin, 1965) and is easily understood through physical arguments. Consider a generator in which the velocity is not constant. The pressure gradient and current density are everywhere linear functions of the velocity, but the dissipation is proportional to the square of the current density. Consequently, in the neighborhood of a nonuniform velocity distribution, there is another distribution with the same integrated total current and pressure drop, but with less internal dissipation. In the zero slip system of this section, Joule losses are the only losses, and the most efficient generator is therefore a constant velocity system.

By fixing the velocity u and treating A(x) as an unknown, the system of equations (3.6), (3.7), (3.8) and(3.9), noticing (5.1), can be reduced to a single nonlinear first order differential equation for A(x) giving a constant velocity distribution. We find

$$\frac{1}{f\left[\frac{1}{A^*}\right]} \; (A^* - 1)^{-2} \; \frac{dA^*}{d\xi} \; = \; 1 \qquad (5.2)$$

where

$$\xi = \frac{ku\sigma_L B(E+uB)}{q_G} \quad x \tag{5.3}$$

is the dimensionless channel coordinate, and where

$$A^* = \frac{Au\rho_L}{q_L} \tag{5.4}$$

is the dimensionless area.

Equation (5.2) has closed solutions for a number of function forms for $f(1-\alpha)$ of expression (3.9).

In case of $f(1-\alpha) = (1-\alpha)^2$, i.e.

$$\sigma = \sigma_L (1-\alpha)^2 \tag{3.10}$$

which is the relationship used in the modeling of the LT-3 generator in Chapter 3 and in the evaluation of experiments with this generator at Argonne National Laboratory, one obtains:

$$(A^*-1) + 2\ \ell n \frac{A^*-1}{2} - \frac{1}{A^*-1} = \xi + C \tag{5.5}$$

where C is a constant of integration.

In case of a different choice:

$$f(1-\alpha) = 1-\alpha \tag{5.6}$$

we find

$$\ell n\ (A^*-1) - \frac{1}{A^*-1} = \xi + C \tag{5.7}$$

while for the case:

$$f(1-\alpha) = (1-\alpha)^3 \tag{5.8}$$

we find

$$1/2\ (A^*-1)^2 + 3(A^*-1) + 3\ \ell n \frac{(A^*-1)}{3} - \frac{1}{A^*-1} = \xi + C \tag{5.9}$$

These relationships are plotted in Figure 5.5 with the integration constants having been adjusted so that $A^*[\alpha] = 2$ for each of the conductivity models. The void fraction α is related to A^* by

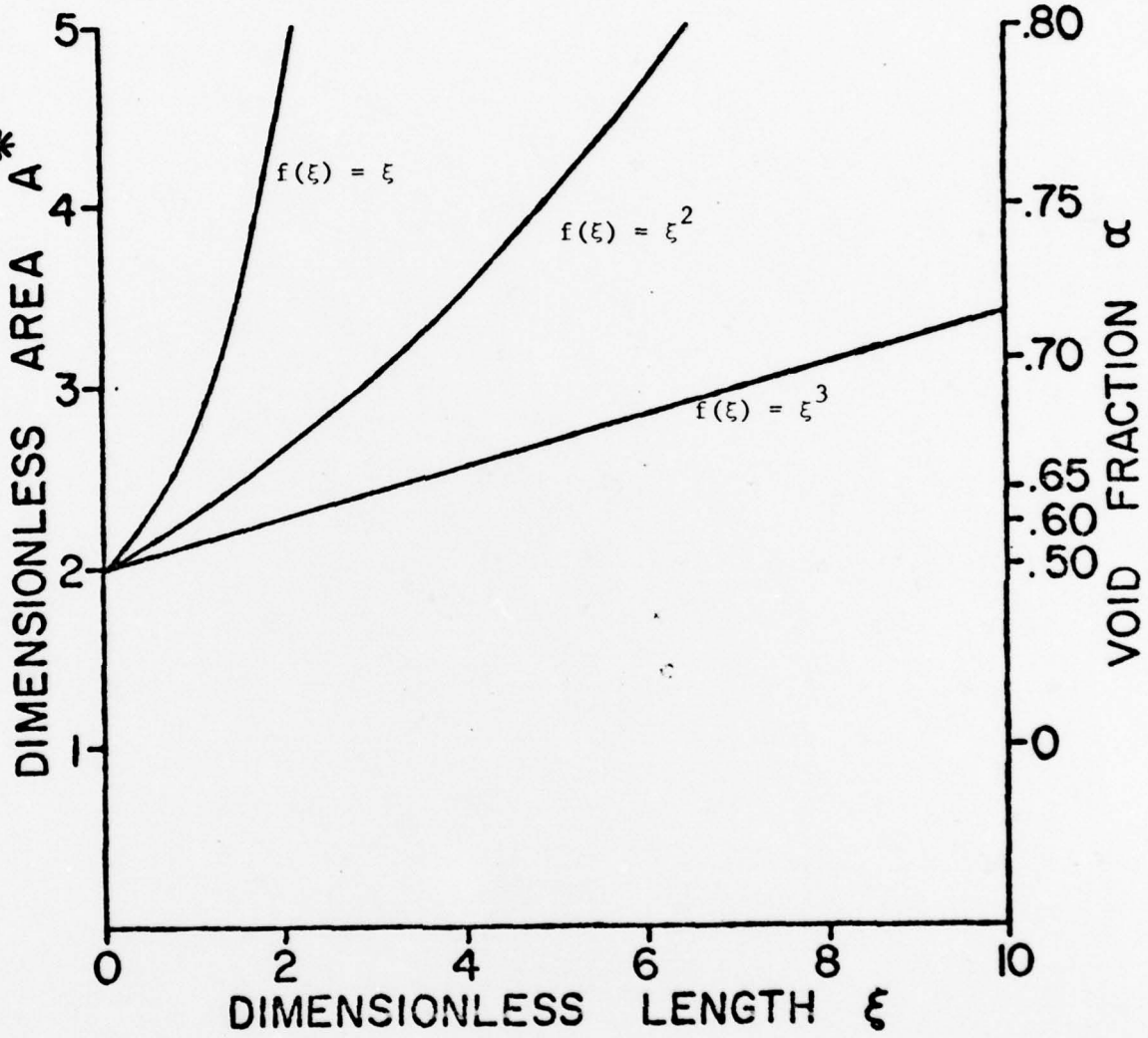

Figure 5.5- Dimensionless area and void fraction versus dimensionless length in constant velocity generator channel.

$$\alpha = \frac{A^*-1}{A^*} \tag{5.10}$$

and is marked on the right ordinate of these figures. Note that, since the distance between electrodes is constant, the curves of Figures 5.5 correspond to the shapes of no slip, constant velocity generators for given conductivity models. Further, a constant velocity generator operating between two given void fractions and with one of the above conductivity models, is similar in shape to the appropriate segment of one of these curves. Note that the channel with the linear conductivity model flares more rapidly than that with the square law model, which in turn flares more rapidly than the channel with the cube law model. This reflects a decreasing Lorentz force in the respective models for given velocity and void fraction.

If the void fraction does not change much over the length of the generator, then a constant velocity channel can be approximated by a channel of linearly varying area. In Figure 5.2 at the peak gross efficiency for a magnetic flux density of 1.8 Tesla, for example, the velocity was found to vary by only two percent over the length of the generator.

REFERENCES

Amend, W., Cole, R., Cutting, J., Pittenger. L.; Annual Report on Experimental Two-Phase Liquid-Metal Magnetohydrodynamic Generator Program, Argonne National Laboratory, ANL/ENG-73-02, (Jun 1973).

Elkins, R.E., Kurzweg, U.H., Trovillion, T.A. and Lindgren, E.R.; Two Phase Hartmann Flows in the MHD Generator Configuration, Department of Engineering Sciences, University of Florida, Technical Report NR 01-100, (Feb 1978).

Holt, E. and Haskell, R.; Plasma Dynamics, The MacMillan Company. 1965.

Hooker, H. and Popper, G.; A Gamma-Ray Attenuation Method for Void Fraction Determinations in Experimental Boiling Heat Transfer Facilities, AEC Research and Development Report, Argonne National Laboratory 5766, (Nov 1958).

Hughes, W.F. and Young, F.J.; The Electrodynamics of Fluids, John Wiley and Sons, Inc., New York 1966.

Jackson, W.D.; Liquid-Metal Faraday-Type MHD Generators, IEEE Transactions, Power Apparatus and Systems, vol. 82, p. 904, (1963).

Medin, S.A.; Variational Problem of Flow in the Channel of an MHD Generator, Teplofizika Vysokikh Temperatur, vol. 3, no. 4, p. 639, (1965).

Petrick, M., Amend, W., Pierson, E. and Hsu, C.; Investigation of Liquid-Metal Magnetohydrodynamic Power Systems, Argonne National Laboratory, Annual Report, ANL/ETD-70-12, (Dec 1970).

Petrick, M., Fabris, G., Cole, R., Hantman, R., Pierson, E. and Cutting, J.; Experimental Two-Phase Liquid-Metal Magnetohydrodynamic Generator Program, Argonne National Laboratory, Annual Report, ANL/ENG-76-04, (Nov 1976).

Petrick, M., Fabris, G., Pierson, E., Curl, D., Fischer, A., and Johnson, C.; Experimental Two-Phase Liquid-Metal Magnetohydrodynamic Generator Program, Argonne National Laboratory, Engineering Division Report, ANL/MHD-77-3. (Sept 1977).

Petrick, M., Fabris, G., Pierson, E., Fischer, A. and Johnson, C.; Experimental Two-Phase Liquid-Metal Magnetohydrodynamic Generator Program, Argonne National Laboratory, Annual Report, ANL/MHD-78-02, (May 1978).

Shercliff, J.A.; The Current-Content of Hartmann Layers, Zeitschrift fur Angewandte Mathematik und Physik, vol. 28, p. 449, (1977).

Trovillion, T. A., Kurzweg, U. H., Elkins, R. E. and Lindgren, E. R.; Two-Dimensional Hartmann Flows of Fluids with Cross-Stream Dependent Electrical Conductivity, The Physics of Fluids, vol. 22, p. 843, (1979).

Wallis, G. B.; One-Dimensional Two-Phase Flow, Mcgraw-Hill, 1969.

Yakhot, A. and Levin, A.; Attenuating the Transverse Edge Effect in MHD Generators, AIAA Journal, vol. 16, no. 11, p. 1203, (1978).

Zuber, N. and Findlay, J.; Average Volumetric Concentration in Two-Phase Flow Systems, Journal of Heat Transfer, p. 453, (Nov 1965).

APPENDIX 1

Documentation of APL program

The functions of this appendix comprise a one dimensional model of a frictionless, massless two phase Faraday generator. The following globals must be specified:

MDL	liquid mass flow rate
MDG	gas mass flow rate
VOLT	terminal voltage
WIDTH	distance between electrodes
B	magnetic flux density
SIGMA	liquid electrical conductivity
PRESO	inlet pressure
RHOL	liquid mass density
K	ratio of gas mass density to pressure
GAM	surface tension
NCD	incremental step down channel

In addition, functions must be specified to give channel area as a function of downstream position (ARF), dispersed liquid conductivity as a function of void fraction (SIG), and void fraction as a function of pressure (ALF). The channel length is specified implicitly in line [8] of CHANNEL in generating the vector

$$(4 \times N)\ \rho'\ \text{NXT}\ b' \qquad \text{(A1.1)}$$

where N is equal to the channel length divided by NCD. The form listed here for ALF iterates to balance the Lorentz force with the force due to phase slippage according to the slip model discussed in Chapter 3.

The assignment

$$R \leftarrow \div 1 + PRS \times CL \div CG \qquad (A1.2)$$

will result in a zero slip model if used for ALF.

Running CHANNEL results in an output of those parameters listed in lines [19] through [25] and in a table consisting of those parameters listed in line [27] for each incremental step down the channel. CHANNEL can also be run for variable channel width and flux density by specifying WIDTH and B as vectors of appropriate length.

APPENDIX 2

Table of Fredholm kernel for averaging Ampere's law for the compensated LT-3 Faraday generator at Argonne National Laboratory. $\left[K(\xi',\xi), \xi = \frac{x}{\ell}\right]$

$24\frac{x'}{\ell}\downarrow$ \ $24\frac{x}{\ell}\rightarrow$	0	1	2	3	4	5	6	7
0	-6.023	-1.264	-.547	-.288	-.161	-.088	-.042	-.011
1	1.408	.077	-1.289	-.565	-.303	-.174	-.100	-.053
2	.678	1.408	.061	-1.320	-.590	-.324	-.194	-.119
3	.408	.673	1.410	.048	-1.349	-.612	-.343	-.211
4	.274	.403	.671	1.416	.038	-1.374	-.630	-.359
5	.196	.270	.401	.672	1.423	.030	-1.397	-.647
6	.146	.193	.267	.400	.674	1.432	.024	-1.418
7	.113	.143	.190	.266	.400	.678	1.442	.019
8	.088	.110	.141	.189	.265	.401	.682	1.453
9	.070	.086	.108	.139	.187	.265	.402	.686
10	.056	.068	.084	.106	.138	.186	.265	.404
11	.045	.054	.066	.082	.104	.136	.185	.265
12	.036	.043	.052	.064	.080	.102	.135	.185
13	.028	.033	.040	.050	.062	.078	.101	.134
14	.021	.025	.031	.038	.047	.059	.076	.099
15	.014	.018	.022	.028	.035	.044	.057	.073
16	.008	.011	.014	.019	.024	.032	.041	.053
17	.002	.004	.007	.010	.015	.020	.028	.037
18	-.005	-.004	-.001	.002	.005	.010	.015	.022
19	-.013	-.011	-.010	-.007	-.005	-.001	.003	.009
20	-.022	-.021	-.020	-.018	-.016	-.013	-.010	-.005
21	-.034	-.033	-.032	-.031	-.029	-.027	-.024	-.021
22	-.048	-.048	-.047	-.046	-.045	-.044	-.042	-.039
23	-.066	-.066	-.066	-.065	-.065	-.064	-.062	-.061
24	-.077	-.078	-.078	-.078	-.078	-.077	-.076	-.075

Table A2.1- Numerical kernel $K(\xi',\xi)$ used for evaluation of equation 4.6. (Continued on next two pages.)

Continued

$24\frac{x'}{\ell}\downarrow$ \ $24\frac{x}{\ell}\rightarrow$	8	9	10	11	12	13	14	15
0	.011	.028	.041	.051	.059	.065	.071	.076
1	-.022	.000	.017	.029	.039	.047	.054	.060
2	-.072	-.041	-.018	-.002	.011	.020	.028	.035
3	-.136	-.089	-.057	-.034	-.018	-.005	.004	.012
4	-.226	-.149	-.102	-.069	-.047	-.030	-.018	-.008
5	-.372	-.237	-.160	-.112	-.079	-.057	-.040	-.027
6	-.661	-.383	-.247	-.169	-.120	-.087	-.065	-.048
7	-1.438	-.674	-.394	-.256	-.177	-.128	-.095	-.071
8	.014	-1.457	-.687	-.403	-.264	-.184	-.134	-.101
9	1.463	.010	-1.476	-.699	-.412	-.271	-.191	-.140
10	.691	1.475	.007	-1.494	-.711	-.421	-.278	-.197
11	.406	.695	1.486	.003	-1.512	-.722	-.429	-.285
12	.265	.407	.700	1.497	.000	-1.529	-.734	-.438
13	.184	.265	.409	.705	1.508	-.003	-1.547	-.746
14	.132	.183	.265	.410	.709	1.518	-.007	-1.565
15	.096	.130	.181	.264	.412	.714	1.528	-.011
16	.070	.093	.127	.179	.263	.412	.717	1.538
17	.049	.066	.090	.124	.177	.261	.412	.720
18	.032	.044	.061	.085	.120	.173	.259	.410
19	.016	.025	.038	.055	.079	.114	.168	.254
20	.000	.008	.017	.030	.047	.071	.106	.160
21	-.017	-.011	-.004	.005	.018	.035	.060	.095
22	-.036	-.032	-.027	-.020	-.010	.002	.019	.044
23	-.059	-.056	-.052	-.046	-.040	-.030	-.018	-.001
24	-.074	-.071	-.069	-.065	-.060	-.053	-.044	-.031

Table A2.1- Continuation of numerical, $K(\xi',\xi)$, kernel for evaluation of equation 4.6. (Continued on next page).

Continued

$24\frac{x'}{\ell}\downarrow$	$24\frac{x}{\ell}\rightarrow$ 16	17	18	19	20	21	22	23	24
0	.080	.084	.087	.091	.093	.096	.099	.101	.103
1	.065	.069	.072	.076	.079	.081	.084	.086	.088
2	.040	.045	.049	.052	.055	.058	.061	.063	.065
3	.018	.024	.028	.032	.035	.038	.041	.043	.045
4	.000	.006	.011	.016	.019	.022	.025	.028	.030
5	-.018	-.010	-.004	.001	.006	.009	.012	.015	.018
6	-.035	-.025	-.018	-.011	-.006	-.002	.002	.005	.007
7	-.054	-.042	-.032	-.024	-.018	-.013	-.009	-.005	-.002
8	-.077	-.060	-.047	-.038	-.030	-.023	-.018	-.014	-.011
9	-.106	-.083	-.066	-.053	-.043	-.035	-.029	-.023	-.019
10	-.146	-.112	-.088	-.070	-.057	-.047	-.039	-.033	-.028
11	-.203	-.151	-.117	-.093	-.075	-.062	-.052	-.044	-.038
12	-.292	-.209	-.156	-.122	-.097	-.080	-.066	-.056	-.048
13	-.446	-.299	-.215	-.162	-.127	-.102	-.084	-.071	-.061
14	-.757	-.455	-.306	-.221	-.168	-.132	-.107	-.089	-.076
15	-1.583	-.769	-.464	-.314	-.228	-.174	-.138	-.113	-.095
16	.016	-1.601	-.782	-.474	-.322	-.235	-.181	-.144	-.119
17	1.546	.021	-1.620	-.795	-.484	-.331	-.243	-.188	-.151
18	.721	1.553	-.028	-1.641	-.810	-.496	-.341	-.252	-.197
19	.408	.721	1.559	-.036	-1.662	-.826	-.509	-.352	-.263
20	.248	.403	.719	1.562	-.046	-1.686	-.844	-.525	-.366
21	.150	.238	.394	.714	1.562	-.060	-1.713	-.866	-.544
22	.080	.135	.223	.381	.703	1.557	-.078	-1.745	-.893
23	.024	.060	.115	.205	.364	.689	1.548	-.101	-1.781
24	-.014	.011	.047	.103	.193	.354	.681	1.546	5.992

Table A2.1- Continuation of numerical kernel, $K(\xi',\xi)$ for evaluation of equation 4.6.